A Raman lidar at Maïdo Observatory (Reunion Island) to measure the water vapor in the troposphere and lower stratosphere: calibration and validation

Hélène Vérèmes[(1,2)], Guillaume Payen[2], Philippe Keckhut[3], Valentin Duflot[(1,2)], Jean-Luc Baray[4], Jean-Pierre Cammas[(1,2)], Jimmy Leclair de Bellevue[1], Stéphanie Evan[1], Françoise Posny[(1,2)], Franck Gabarrot[2], Jean-Marc Metzger[2], Nicolas Marquestaut[2], Susanne Meier[5], Holger Vömel[6], Ruud Dirksen[5] and Patrice Boissier[7]

[1]Laboratoire de l'Atmosphère et des Cyclones, UMR8105 (CNRS, Université de La Réunion, Météo-France), Saint-Denis de La Réunion, France

[2]Observatoire des Sciences de l'Univers de La Réunion, UMS3365, Saint-Denis de la Réunion, France

[3]Laboratoire ATmosphères, Milieux, Observations Spatiales-IPSL, UMR8190 CNRS, UVSQ, UPMC, Guyancourt, France

[4]Laboratoire de Météorologie Physique, UMR6016, Observatoire de Physique du Globe de Clermont-Ferrand, Université Clermont Auvergne, Clermont-Ferrand, France

[5]Deutscher Wetterdienst, Meteorological Observatory Lindenberg, Lindenberg, Germany

[6]National Center for Atmospheric Research, Boulder, CO, USA

[7]Observatoire Volcanologique du Piton de la Fournaise, IPGP, Sorbonne Paris Cité, UMR 7154 CNRS, Paris, France

Correspondence to: Hélène Vérèmes (helene.veremes@univ-reunion.fr)

Abstract. The Maïdo high-altitude observatory located in Reunion Island (21°S, 55.5°E) is equipped with the Lidar1200, an innovative Raman lidar designed to measure the water vapor mixing ratio in the troposphere and the lower stratosphere. The calibration methodology is based on a GNSS (Global Navigation Satellite System) IWV (Integrated Water Vapor) dataset and lamp measurements. The mean relative standard uncertainty in the transfer of the calibration is around 2.7%. Two years of lidar water vapor measurements from November 2013 to October 2015 are now processed. By comparing CFH (Cryogenic Frost point Hygrometer) radiosonde profiles with the Raman lidar profiles, it is shown that the lidar is able to provide accurate measurements up to 22 km. The ability to measure water vapor mixing ratios of a few ppmv in the lower stratosphere is demonstrated with a 48-hour integration time, a total uncertainty lower than 0.8 ppmv and a relative uncertainty of less than 22%. This Raman lidar is dedicated to providing international networks with regular profiles of water vapor measurements having high vertical resolution and low uncertainties, and to the wider interest of research on stratosphere-troposphere exchange processes and the long-term survey of water vapor vertical distribution in the Southern Hemisphere. A strategy of data sampling and filtering is proposed to meet these objectives with regard to the altitude requested. 10-min time integration and 65-90 m vertical resolution ensure a vertical profile reaching 10 km but more than 2800 minutes and a vertical resolution of 150-1300 m

are necessary to reach the lower stratosphere with an uncertainty of less than 20%.

1 Introduction

To monitor potential climate changes, observations of essential climate variables (ECV), such as atmospheric water vapor (Bojinski et al., 2014), are necessary. The factors influencing the spatiotemporal variability of this greenhouse gas are various: convection, precipitation, temperature (Kennett and Toumi, 2005), transport, and dynamical processes from eddies to synoptic scale events (Vogelmann et al., 2015). The residence time of water vapor in the atmosphere is several days to weeks (Trenberth, 1998; Läderach and Sodemann, 2016). Nevertheless, in the troposphere, its temporal and spatial variability can be high at a scale of dozens of minutes and less than one kilometer (Vogelmann et al., 2011, 2015). It is noteworthy that the variability of the water vapor in the upper troposphere (UT) is considerably higher than in the lower stratosphere (LS). Water vapor is a challenging ECV to measure in the UT/LS (Upper Troposphere/Lower Stratosphere) (GCOS, 2003), which is a key zone of exchanges between the troposphere and the stratosphere (Holton et al., 1995) and should be monitored.

Long-term series allow the international community to make progress on important climatological issues, such as the contributions of stratospheric water vapor to decadal changes in the rate of global warming (Solomon et al., 2010). Networks ensure the broadcasting of such data. Selection criteria are important for certification within the networks. These criteria include: high-quality, long-term stability, regularity, and detailed metadata including a complete uncertainty budget. This last exercise is carried out through a strict examination of the data processing algorithms and calibration methodologies. This rigor is essential to monitor the atmosphere and climate changes efficiently (Immler et al., 2010), especially in the case of UT/LS water vapor. To track, monitor and set water vapor trends globally from the troposphere up to the lower stratosphere, it is essential that dense, regular measurements supply global networks, specifically NDACC (Network for the Detection of Atmospheric Composition Change; Kurylo and Solomon, 1990) and GRUAN (GCOS Reference Upper Air Network; Seidel et al., 2009, Bodeker et al., 2015). The NDACC community focuses strongly on the study of the dynamics and chemical processes taking place in the UT/LS. One of the scientific goals of GRUAN is the characterization of the water vapor variability and trends in the troposphere and, more specifically, in the UT/LS (Seidel et al., 2009).

In order to obtain reliable water vapor trend detection in the UT/LS and process studies, GRUAN has specific requirements that are summarized in Table 1. The concept of monitoring trends in the upper troposphere is different from doing it in the lower stratosphere. Boers and Meirgaard (2009) and Whiteman et al. (2011a) show that decades are necessary to detect trends in the UT. To detect such trends, a high random uncertainty (up to 50%, Table 1) can be acceptable if a high-frequency measurement schedule is set up (Whiteman et al., 2011a). Some measurement and calibration procedures should be implemented in order to randomize the sources of systematic uncertainty (Whiteman et al., 2011a) and this systematic uncertainty should remain between 5 and 10% (Table 1). Measurements performed twice a week would constitute a good compromise between logistical costs and the time for detection (Whiteman et al., 2011a). The requirements on the systematic uncertainty and high stability are the same whether UT or LS water vapor trends are considered. The variability of the stratospheric water vapor being much lower than that of tropospheric water vapor, the related measurements need to be much more accurate in the lower stratosphere than in the upper troposphere. The recommended random uncertainty should not exceed 10% (Table 1). The requirement on the stability is

0.3%/decade (GCOS, 2009). The desired stability for time series of water vapor in the lower stratosphere is better than 2% per year (GCOS, 2009). To detect trends in both the UT and the LS, day and night samplings should be effective (GCOS, 2013). Investigation of process studies is another scientific objective, which has different measurement needs. A systematic error of 10% is adequate (Table 1). A guideline of 10 to 25% is given by GCOS for the random uncertainty (Table 1). For such investigations, each case can be unique and the random uncertainty will depend on the individual needs. Considering that the time scale of the different studies is generally short, calibration stability is not the main concern (GCOS, 2013). Nevertheless, high vertical and temporal resolution is needed (10-100 m for a 1-min integration, Table 1). Day and night-time, or even continuous, measurements should be performed by the instruments. For studies such as stratosphere-troposphere exchanges (STE), the probed column should reach the tropopause, or even the LS in the case, for example, of deep convection. GCOS report n°171 states that these requirements are based on research goals, and that they “may not be currently achievable” (GCOS, 2013).

Water vapor measurement techniques are various: in situ or remote sensing, ground-based, airborne or space based (Wulfmeyer et al., 2015) but a limited number of instruments are able to accurately measure the vertical distribution of water vapor in the UT/LS. Sondes with a capacitive sensor are not sufficiently reliable in the stratosphere (WMO, 2011) and few of these sondes can measure the water vapor in the subtropical upper troposphere. Among the radiosonde sensors measuring humidity, frost point hygrometers are the most accurate. The CFH (Cryogenic Frost point Hygrometer) exhibits an accuracy of better than 4% in the tropical lower troposphere, 9% around the tropopause and about 10% at 28 km (Vömel et al., 2007). Nevertheless, CFH are rarely launched on a routine basis at atmospheric observatories, mainly because of their cost. GRUAN recommends launching a radiosonde with a CFH or similar sondes at least once per month (Bodeker et al., 2015). Regarding satellite measurements with global coverage, the MLS (Microwave Limb Sounder) is very accurate (Read et al., 2007). Between 100 and 121 hPa, the accuracy (bias) of the MLS is around 15-20% (8-12%). At 83 hPa, it is reduced to 10% (7%). The detection threshold is extremely low: 0.1 ppmv above 150 hPa (Livesey et al., 2011). Few of the other space borne sensors currently operating show comparable performance for water vapor measurement in the vicinity of the tropopause and in the lower stratosphere. Although the accuracy of MLS is very high, its horizontal resolution is more than 165 km and its vertical resolution is of the order of 2-3 km. It is noteworthy, however, that Hurst et al. (2016) found some divergence between MLS and balloon-borne frost point hygrometers exceeding the accuracy of both instruments. Water vapor vertical distribution can also be measured by two lidar techniques: DIAL (DIfferential Absorption Lidar) and Raman lidar. An overview of the capacities of the ground-based DIAL lidar by Wulfmeyer et al. (2015) reports that they have a range of 10 km (for night measurements) with a vertical resolution from 15 to 900 m and an accuracy of 1 to 10% (depending on the altitude). No calibration factor is needed, avoiding supplementary uncertainty. Nevertheless, the DIAL measurement is limited in altitude because of the large absorption in the lower troposphere in cases of high water vapor content (Turner et al., 2000).

In contrast, some ground-based NDACC Raman lidars are able to reach the UT/LS; they include the Purple Crow Lidar (Canada; Argall et al., 2007), the Table Mountain Facility Lidar (United-States; Leblanc et al., 2012) and the Tor Vergata system (Italy; Dionisi et al., 2010) lidars. The altitude of the tropopause is lower in such mid-latitude areas than in the (sub)tropics. The Mauna Loa Observatory Raman lidar is able to reach 15 km on a routine basis (Barnes et al., 2008). Raman lidar may be able to measure water vapor in the tropical UT/LS but such performances remain to be demonstrated and quantified precisely. The calibration of the data of Raman lidars is important for the stability of the measurement on a short- and long-term basis (Sherlock et al., 1999a) and can be calculated using two different methods. The first consists in using a complementary water vapor measurement, and the calibration therefore depends on the accuracy of another instrument. It is also possible to make an independent determination: different relevant parameters of the system are measured or calculated experimentally (Sherlock et al., 1999a, Venable et al., 2011). Whatever the method used, the calibration determination will induce an uncertainty of at least 5% (Wandiger et al., 2005). Calibration is typically performed using external water vapor profiles from radiosoundings (Sherlock et al., 1999a). Nevertheless, all fixed NDACC Raman water vapor lidars use Vaisala sondes to calibrate their database. It is noteworthy that an independent calibration (Venable et al., 2011) is performed for the ALVICE (Atmospheric Lidar for Validation, Interagency Collaboration and Education), a mobile lidar. Regarding the dependent calibration, different measurements have been tested and compared to calibrate the data (GNSS, radiometer and optimized matching methods when using radiosoundings) during different campaigns: DéMéVap (Développements Méthodologiques pour le sondage de la Vapeur d'eau dans l'atmosphère; Bock et al., 2013), MOHAVE (Measurements Of Humidity in the Atmosphere and Validation Experiments; Leblanc et al., 2012), and HOPE (HD(CP)² Observational Prototype Experiment; Foth et al., 2015). The uncertainty on the calibration factor calculated by the different instruments was between 5 and 10%. One conclusion of these studies is that the GNSS IWV (Integrated Water Vapor) is suitable to calibrate the Raman lidar, the resulting uncertainty being around 7% during DéMéVap (Bock et al., 2013). The key question when using the GNSS IWV for the calibration of Raman lidar water vapor measurements is the lidar's ability to retrieve the total water vapor column to ensure that the same columns are probed by the two instruments; in other words: whether or not the lidar is able to measure water vapor close enough to the ground.

In Reunion Island, a new Raman lidar has been designed to simultaneously monitor the water vapor from the ground up to the lower stratosphere and the temperature in the stratosphere and the mesosphere. The system is an updated version of the former Rayleigh-Mie-Raman system in operation at Saint-Denis (Reunion Island) between 2002 and 2010. In October 2012, the new lidar system was set up at a higher altitude, at the Maïdo facility located at 2160 m asl (Baray et al., 2013). At the same time, most of the instruments of the OPAR (Observatoire de Physique de l'Atmosphère de la Réunion) moved to the observatory. In order to optimize the instrument configuration and to evaluate a first set of data, two measurement campaigns were organized: MALICCA-1 (MAïdo LIdar Calibration CAmpaign) in April 2013 (Keckhut et al., 2015) and MALICCA-2 in November 2013. The MALICCA-1 dataset shows good agreement between the water vapor data measured by the lidar and those measured by the other instruments (Vaisala RS92, MLS, Dionisi et al., 2015). The relative difference between the lidar profiles and 15 simultaneous radiosoundings (Vaisala RS92) is lower than 10% for the lower and middle troposphere and between 10 and 20% for the upper troposphere. Two integration methods have been tested: 240 minutes leading to an uncertainty of 2 ppmv between 17 and 20 km, and a monthly integration (i.e. an integration of ~ 1920 min) leading to an uncertainty of 1 ppmv at 20 km, which demonstrates the ability of the lidar to measure quantities of only a few ppmv in the UT/LS (Dionisi et al., 2015). The monthly mean profile of water vapor based on MLS data agrees well with the mean lidar profile of MALICCA-1 in the lower stratosphere. The main conclusions of Dionisi et al. (2015), based on two weeks of intensive measurements, need to be reviewed using a longer, 2-year, period of routine measurements. GNSS data can be used to calibrate the water vapor mixing ratio profiles but it is still necessary to develop a robust methodology for long-term calibration, as required for participation in international networks such as NDACC, particularly as this Maïdo Raman water vapor lidar (called hereafter "Lidar1200") has recently been provisionally affiliated with the NDACC. The affiliation will become conclusive when absence of fluorescence and a stable calibration method are both demonstrated using validation campaigns involving frost point hygrometer measurements.

The main objectives of the present paper are to assess the ability of this lidar to monitor the water vapor in the upper troposphere and in the lower tropical stratosphere on a long-term basis and to introduce its 2-year dataset of water vapor profiles. We will describe the instrument, the data processing and the calibration methodology. A routine calibration methodology, based on GNSS observations, has been developed in order to improve the reliability of the calibration coefficient and the robustness of the measurements. This methodology is detailed in Sect. 2. The validation of the profiles by comparing the lidar data with CFH radiosoundings will be presented in Sect. 3. The performances of the instrument are evaluated in detail in Sect. 4, from the detection of fine-scale structures to the potential establishment of climatologies and then trends in the UT/LS. Finally, an overview of the 2-year dataset is given (Sect. 5).

2 Description of the system, the data processing and the calibration methodology

2.1 The Raman system on a routine basis

Before being transferred to the Maïdo Observatory in 2012, the Raman water vapor lidar operated at sea level in the north of Reunion Island, at Saint-Denis (Hoareau et al., 2012). Some critical points have been handled (fluorescence, power and parallax effects) in order to optimize the new configuration of the system (Sherlock et al., 1999b; Hoareau et al., 2012). The system has been upgraded to work at 355 nm, a more efficient wavelength than 532 nm (Dionisi et al., 2015). Laser pulses are generated by two Quanta Ray Nd:Yag lasers with a repetition rate of 30 Hz. The use of two lasers significantly increases the power of the signal. They are synchronized through a pulse generator cube with an uncertainty of less than 20 ns. The emitting pulse of each laser has an energy of 375 mJ.pulse^{-1} and a duration of 9 ns and they are brought together through a polarization cube. The geometry for transmitter and receiver is coaxial for three reasons: i) to avoid parallax effects, ii) to extend the measurements down to the ground and iii) to facilitate the alignment. The backscattered signal is collected by a Newtonian telescope with a primary mirror 1.2 m in diameter. When collecting small Raman scattering by water vapor compared with the large elastic scattering able to generate fluorescence, the use of an optical fiber is an important issue. It has been shown that the fluorescence in such cables can cause systematic biases (Sherlock et al., 1999b). Thus, no optical fiber is employed. An optical box unit is used directly after the telescope to separate the Raman and Rayleigh signals. Thanks to a diaphragm field stop at the entrance of the separation unit, the field of view (FOV) of the system is adjustable (from 3.0 to 0.5 mrad). On a routine basis, a 2 mm FOV (0.5 mrad) allows the background light to be reduced and limits photo-counting saturation from low altitude scattering. The overlap factor is quite similar for both channels. Thus, water vapor profiles can be retrieved down to the ground. Details on the different tests run during MALICCA that led to the final choice of the operational optical configuration are given in Dionisi et al. (2015). The separation unit is composed of dichroic beam splitters and interference filters, which separate the backscattered light. Hamamatsu miniature PMT and Licel transient recorders are used for the photo detection and data acquisition in photon counting.

2.2 Water vapor data processing

2.2.1 Water vapor mixing ratio retrieval equation

The initial data processing algorithm (Dionisi et al., 2015) has been upgraded to version 2.4.0 to include identification and quantification of the uncertainties and determination of the vertical resolution. The equation to retrieve the water vapor mixing ratio (WVMR) is based on:

$$WVMR(z) = C.O(z).F(z).\frac{P_{H2O}(z) - b_{H2O}(z)}{P_{N2}(z) - b_{N2}(z)} \Delta\tau(z) \qquad (1)$$

where C is the calibration coefficient, $O(z)$ is the overlap factor, $F(z)$ is the temperature dependence of the Raman cross-section, $P_i(z)$ is the number of photons received by the detector for i (with i=H_2O or N_2), $b_i(z)$ is the sky background, and $\Delta\tau(z)$ is the differential term due to the atmosphere.

The number of photons received by the detector might not correspond to the real number of photons, in particular when this number is high and the detector is saturated. A non-paralyzable photon counting formula is used to desaturate the signal:

$$P_i = \frac{R_i}{1 - \tau_i \dfrac{c}{2.\delta z.L} R_i} \qquad (2)$$

where R_i is the number of photons counted by the detector, τ_i the dead-time parameter of the detector, c the speed of light, δz the space resolution, and L the number of shots of the laser. The saturation affects mainly the N_2 channel; its impact on the H_2O channel is very weak.

2.2.2 Identification and quantification of the uncertainties

A detailed analysis to identify the sources and quantify the different uncertainties has been carried out. We assume that all the parameters of Eq. (1) are independent. The total absolute uncertainty (u_{WVMR}) on the calibrated profiles ($WVMR$) is calculated as follows:

$$\frac{u_{WVMR}}{WVMR} = \sqrt{\frac{u_C^2}{C^2} + \frac{u_O^2}{O^2} + \frac{u_F^2}{F^2} + \frac{\left(u_{P_{H2O}}^2 + u_{b_{H2O}}^2\right)}{\left(P_{H2O} - b_{H2O}\right)^2} + \frac{\left(u_{P_{N2}}^2 + u_{b_{N2}}^2\right)}{\left(P_{N2} - b_{N2}\right)^2} + \frac{u_{\Delta\tau}^2}{\Delta\tau^2}} \qquad (3)$$

where u_i is the uncertainty on i depending on the altitude z. The different sources of the assumed uncorrelated statistical uncertainty are associated with the counting of the number of photons collected by the detector for the water vapor and nitrogen channels (depending on the altitude). The main sources of systematic uncertainties are the determination of the calibration coefficient, the temperature-dependence of Raman backscattering, overlap function ratios and the differential transmission in the atmosphere at the wavelengths of the water vapor and nitrogen Raman channels. The uncertainty due to the dead-time in the desaturation is estimated to be less than 1% at 4 km and is neglected. Optical tests evaluating the uncertainty associated with the contamination of the signal by fluorescence concludes that, if there is any, the bias is negligible (Dionisi et al., 2015). Considering that there are few background aerosols and turbid conditions above Reunion Island, and assuming that the differential transmission due to aerosols is much smaller than the differential transmission due to molecules, the uncertainty on the retrieval due to aerosols is neglected.

The total uncertainty budget of the Lidar1200 water vapor profiles includes the following uncertainties (Fig. 1):

- Uncertainty due to the detectors (PMT), which is a statistical uncertainty and follows a Poisson distribution. It is calculated by the square root of the signal. It increases with the altitude and depends on the filter used.
- Uncertainty of the background noise, which is calculated as the variance of the background noise divided by the square root of the number of points.
- Uncertainty on the differential absorption, which is driven by the uncertainty on the extinction of the molecules. The atmospheric density profile is calculated with a model of atmospheric density having an arbitrary uncertainty fixed at 15% on this profile. After propagation of the uncertainty, it represents a negligible value of only 0.05% on the data at 20 km asl.
- Uncertainty on the calibration, which is a combination of the uncertainties on the external source of measurement and the transfer of the calibration source to the lidar profile (see Sect. 2.3.6 for more details). The accuracy of the GNSS IWV measurement is about 1 mm, varying from 6% to 18%, depending on the season and the total water vapor content (Sect. 2.3.1). The uncertainty of the transfer of the calibration is estimated to be less than 3%.
- Uncertainty due to the temperature-dependence of the signal, which is estimated to be maximum at the tropopause, at 6.7% (Whiteman et al., 2003).
- Uncertainty due to the overlap factor is estimated to be 4% at the ground and to decrease up to the maximum recovery altitude of the signal.

The total uncertainty is directly influenced by the calibration and the quality of the measurements. It varies because of the statistical and systematic errors in the lower troposphere. In the middle troposphere up to the lower stratosphere, the statistical uncertainties determine the reliability of the profiles. The uncertainty depends strongly on the integration time and the filtering of the signal. Thus, it is important to use a suitable filter regarding the vertical resolution and the order of magnitude of the total uncertainty.

2.2.3 Vertical resolution

The vertical resolution of the raw data is 15 m. Data are smoothed with a low-pass filter using a Blackman window; thus, the final resolution is different from the initial resolution. The number of points of the filter increases with the altitude to compensate for the signal-to-noise ratio (SNR) decrease. The NDACC has formulated and adopted two standardized definitions for the calculation of the final vertical resolution for its lidars, based on 1) cut-off frequency of digital filters (used here) or 2) the full-width at half-maximum of a finite impulse response (Leblanc et al., 2016). Based on the number of points used for the filter to vertically average the data, the vertical resolutions (Fig. 2) that can be derived from these definitions are 100-200 m in the lowest layers, 500 m in the mid-troposphere, 600 m in the upper troposphere and 700-750 m in the lower stratosphere, for a filter using the Blackman coefficients reaching 121 points at 20 km asl.

To summarize, the uncalibrated profiles are processed with a vertical resolution and an integration time, both depending on the water vapor variability at several levels. In order to convert the backscattered radiation profiles into water vapor mixing ratio profiles, it is necessary to calculate a calibration coefficient from water vapor column ancillary data afterward. The specific calibration methodology that has been developed for the Lidar1200 is described in the next subsection. The validation and evaluation of the performances of the lidar is detailed in Sect. 3 and 4.

2.3 Calibration methodology

2.3.1 The GNSS technique

The GPS and GLONASS (GLObal NAvigation Satellite System) satellite constellation signals are collected by a ground-based receiver. With respect to propagation in a vacuum, the signal traveling between a GPS satellite (altitude of 20,200 km) and a ground-based receiver is delayed by atmospheric constituents (dry air, water vapor, clouds, hydrometeors and aerosols) and is affected by the temperature. To determine the IWV from GNSS data, the atmospheric zenith total delay (ZTD) is estimated. Using surface pressure information, the ZTD can be divided into a hydrostatic term, i.e. the Zenith Hydrostatic Delay (ZHD or so-called dry delay) calculated through the Saastamoinen formula (Saastamoinen, 1972) and the Zenith Wet Delay (ZWD, so called wet delay). The hydrostatic delay, which is derived by applying the condition that hydrostatic equilibrium is satisfied, depends on the total weight of the atmosphere above. The wet delay is the propagation delay experienced by GPS signals due mainly to water vapor abundance. ZWD is converted into IWV, using surface temperature and empirical formulas (Bevis et al., 1992; Emardson and Derks, 2000). The raw data inversion process and its uncertainty is mainly controlled by mapping the Slant Total Delay (STD, in any direction) to the delay at zenith, to which horizontal gradients (North-South and East-West) are added.

Many authors have assessed the accuracy of GPS IWV, based on comparisons with radiosondes, sun photometers, microwave radiometers, lidars and interferometers (Foelsche and Kirchengast, 2001; Niell et al., 2001; Bock et al., 2016). These techniques agree on about 1-2 $kg.m^{-2}$ for typical values between 5 and 30 $kg.m^{-2}$. In practical terms, an accuracy ranging from 0.5 to 2.5 $kg.m^{-2}$ has been observed depending on the location of the measurements. However, several sources of uncertainty still need to be investigated (Bock et al., 2013).

A TRIMBLE-NETR9 receiver (MAIG) was installed at the Maïdo Observatory in 2013 in order to receive the GNSS data (see http://rgp.ign.fr/STATIONS/#MAIG). The GNSS network used to calculate IWV above the station includes 20 other local stations disseminated over the island and, in order to ensure a sufficiently high number of baselines for the differential data processing using GAMIT software v10.32 (King and Bock, 2007), 15 overseas stations in the Indian Ocean are also included. The typical cutoff elevation angle is fixed at 10° to ensure that the area sounded for water vapor is as local as possible. Currently, the database produces hourly IWV at the Observatory elevation. The uncertainty is in agreement with the literature and is about 1 mm. The total uncertainty of the GNSS IWV is consistent with the description by Ning et al. (2013). The uncertainty in the ZTD represents about 75% of the total GNSS uncertainty, and is a mixture of systematic and statistical uncertainties (Ning et al., 2016). For the MAIG

GNSS IWV > 5 mm and IWV > 10 mm during 2013-2015, the averages of the total uncertainty of the GNSS measurements are around 11% and 7.5%, respectively.

2.3.2 Relevance of the use of GNSS IWV for calibration

The raw data of the Lidar1200 need to be calibrated. Two ancillary measurements could be used: radiosondes or GNSS. The main concern for the calibration is to be able to have collocated, simultaneous measurements on a routine basis. We consider that space-time criteria for collocation do not match when we consider the biweekly normal operation of the Raman lidar (15:00-21:00 UTC) at the Maïdo Observatory and the daily 12:00 UTC radiosounding (Météo-France) or the weekly 10:00 UTC ozone radiosounding (NDACC/SHADOZ OPAR site) based at the airport, which is 20 km from the Maïdo Observatory. Launching two sondes per week from the Maïdo Observatory would have a significant financial and logistical cost. These are the main reasons for choosing the GNSS for the calibration. GNSS measurements are abundant, collocated and simultaneous to the lidar data. IWV is calculated each hour providing that the uncertainty in the ZTD estimated by GAMIT remains below the standard threshold of 30 mm, which occurs around 95% of the time. The other reasons are 1) the independence of the lidar series regarding the radiosounding series, which have revealed some discontinuities in the past due to the relative humidity sensor calibration and change in the equipment decided by the manufacturers, and 2) the hourly availability of the GNSS data. Since 2013, the lidar profiles can be calibrated using integrated water vapor columns obtained from these GNSS measurements, ensuring a better stability of the calibration in the long term. The GNSS raw data are archived and could be reprocessed in case of improvement of the data retrieval algorithm.

As stated earlier, the main prerequisite to the use of GNSS IWV to calibrate Raman lidar water vapor measurements is the ability of the lidar to actually probe the IWV, i.e. to start measurements at ground level. The emission and reception parts being coaxial, the complete overlap altitude of the lidar is very low. The overlap of the laser beam with the field of view of the telescope is partial from the ground (i.e. 2.2 km asl) to 4 km asl. The data processing being based on a ratio between the two channels (H_2O and N_2), the first available point of the lidar water vapor profile is 15 meters above the instrument (vertical resolution of the raw data). This somewhat propitious, but expected, result can be explained by the contribution of the coaxial geometry of the optical design, the FOV, and the diameter of the receiving telescope. One concern regarding the use of total column is that, sometimes, the lidar profile could not reach the lower stratosphere and thus concerned only a partial column. A calculation performed on the vertically averaged water vapor data of the CFH sondes launched during the MORGANE (Maïdo ObservatoRy Gas and Aerosol NDACC Experiment) campaign (Reunion Island, May 2015), shows that, up to 5 km, the cumulated water vapor represents 90% of the total column; above 10 km, 99% of the whole column is contained. Thus, it appears sufficient to use IWV total columns to calibrate the Lidar1200 water vapor profiles when the range of the profile is higher than 10 km.

2.3.3 Description of the methodology

Usually a calibration coefficient is the ratio between a reference instrument, the GNSS IWV here, and the uncalibrated lidar IWV data. In this section, the hourly calibration coefficient, named “hourly coefficient” represents the ratio between the GNSS IWV calculated on a 1-hour window and the lidar IWV integrated over the same temporal extent. The principle can be illustrated as follows: if the GNSS measurement corresponds to 18:00 LT, the lidar data are integrated between 17:31 and 18:30 LT (with a minimum of 45 minutes). For the near-real-time treatment, it remains necessary to check if there are instrumental changes because they might alter the calibration coefficient. At the beginning of each night of measurements, a systematic lamp measurement is made in order to detect potential sudden instrumental changes. The lamp measurement consists in the emission of white light onto the telescope, which illuminates the sensors. An acquisition is launched and the information extracted is "white noise". This noise is averaged over the whole altitude range and for all the channels. Finally, the lamp measurement value corresponds to the ratio of the signal of the Raman H_20 channel and the Raman N_2 channel. This value is independent of the altitude and is impacted by the laser power, losses due to the reception optics, and the efficiency of the sensors. The lamp measurement reveals only the changes that occur on the reception part of the system and this technique has shown some failure modes (Whiteman et al., 2011b). Therefore, in addition to the lamp measurements, the logbook can be checked to reduce non-automatic detections of instrumental changes, especially for the emission part of the system.

The hourly coefficient varies in time, probably because the integration methods are different. Even if the GNSS and the lidar are collocated, they do not measure exactly the same volume of water vapor (in space and in time). With hindsight on the dataset, a manual identification of the periods with a stable hourly coefficient allows the problem of automatic detection of instrumental change to be overcome. Periods of quasi-stationarity of the hourly coefficient can be defined inside periods in which the lidar was considered as instrumentally stable, called IQSPs (Instrumentally Quasi-Stationary Periods). The IQSPs are validated by checking the results of the lamp measurements and the logbook overview. The average hourly coefficient of each IQSP is considered as the "calibration coefficient" of each measurement performed during this period. Some outliers are not taken into account in the calculation of the calibration coefficient: the hourly coefficients for which the GNSS IWV is less than a threshold value (between 5 and 10 mm), considering that the uncertainty is high. At the end of the process, there is only one calibration coefficient for all the data belonging to the same IQSP. Even though the outliers are not included in the calculation of the coefficient, the associated measurement can still be calibrated by using the calibration coefficient of the IQSP. The methodology ensures the calibration of data integrating several nights of measurement inside the same IQSP. The measurement is re-calibrated only at the beginning of each period. Once the IQSPs are identified, the calibration coefficients are calculated, and the data can be calibrated and used for geophysical purposes.

Figure 3 shows the time series of the hourly coefficients (blue circles and crosses) of the Lidar1200 water vapor measurements between November 2013 and October 2015 and the 12 associated IQSPs (delimited by the vertical dotted lines), with lamp measurements superimposed (green dotted line). Analysis of the lamp measurements leads to the identification of one very short quasi-stationary period associated with changes of the calibration coefficient P04 in June 2014 (change of the interference filter of the 407 nm channel). The other changes of IQSP involving a new calibration coefficient were identified thanks to the logbook: change of optical components (such as lenses, diaphragm, etc.), major realignments of the optics of the lidar and interventions on the lasers. The lamp measurement and the identification of the instrumental changes on the emission part of the instrument agree with the delimitation of the IQSPs. The data outliers are based on a threshold of 5 mm, which represents 33% of the GNSS IWV. The calibration coefficients of the 12 IQSPs are listed in Table 2 (corresponding to the horizontal solid red lines in Fig. 3). We recall that the raw water vapor profiles of one period are calibrated with the average hourly coefficient of the IQSP. That means, for example, that the water vapor profiles of 17 November 2014 are calibrated with a ratio of 209, as are all the profiles retrieved using the measurements made between 17 November 2014 and 25 January 2015. The measurements are re-calibrated for the change of period (from P07 to P08), on 26 January 2015 following an important realignment of the optics of the lidar. The 2-year database was calibrated (Table 2) with the exception of two periods (20 May to 8 June 2014 and 11 to 12 May 2015) corresponding to a training session for the technicians and scientists on the alignment of the water vapor lidar, and the last technical preparation for the MORGANE campaign, respectively. It should be noted that there was no data from 1 January to 9 March 2014 and from 9 to 16 April 2015. The calibration coefficient in Table 2 represents the coefficient that was ultimately used to calibrate the Lidar1200 water vapor dataset supplied to the national and international networks. The hourly coefficient shows a standard deviation of 20% over the 2013-2015 period, which is mainly explained by instrument changes. The instrument adjustments yield a variation of the calibration coefficient and the standard deviation of the IQSP calibration coefficients is 17% (Table 2). The standard deviation of the hourly coefficients inside a single IQSP varies between 5 and 16% (depending on the IQSP) with a mean standard deviation of 10%. Several hypotheses could explain the variability of the hourly coefficients: some remaining instability in the instrument, the high variability of tropospheric water vapor, and uncertainties on the external source of measurement for the calibration. The first hypothesis would be the persistence of a small instrumental instability that could be linked to temperature variation or other unknown environmental factors. The impact of persistent instrumental instabilities on the stability of the calibration of water vapor Raman lidar has been recently documented by David et al. (2017) and such instabilities are not specific to the Lidar1200. Even if there were some instabilities, their impact should be small. The other hypotheses are discussed in the next subsection.

Our external source of measurement for the calibration is based on a daily IWV dataset. This is similar to the daily calibration technique used by the Atmospheric Radiation Measurement (ARM) program, which runs its Raman lidar calibration with respect to a microwave radiometer (Turner et al., 2002). Nevertheless, our methodology differs in that it uses IQSP to calibrate all the data of the same period with a single coefficient. The re-calibration is not performed daily but only when it is necessary, i.e. when there is an instrument change. In addition, the lidar profiles that could not have been calibrated without a high uncertainty (coming from the external source of measurement in cases of IWV < 5-10 mm), can be reliably calibrated and used for geophysical purposes.

2.3.4 Comparison with other calibration devices

The previous subsection has shown that the GNSS technique provides a suitable methodology to calibrate the Lidar1200. To evaluate how suitable this methodology is, it was compared with other widely used calibration techniques, in particular the use of radiosoundings. Dionisi et al. (2015) showed encouraging results for the use of GNSS IWV based on a first comparison with the use of Vaisala RS92 for calibrating the profiles during the MALICCA-1 campaign. To evaluate the robustness of the GNSS calibration, the method described above needed to be further investigated on the basis of more comparisons. The MORGANE campaign involving CFH, Vaisala RS92 and RS41 and Modem M10 sondes launched from the Maïdo Observatory concomitantly with GNSS and lidar measurements provided an interesting opportunity. The comparison method was based on a daily calibration of the lidar profiles using a GNSS or a sonde reference profile. The radiosonde-based calibration technique was adapted from Whiteman et al. (2012). Within the height range of 3 to 13 km asl (for the Vaisala and CFH sondes) and 3 to 8 km asl (for the M10 sondes), the algorithm performs a linear regression between the lidar and the radiosonde profiles by segments of 0.6 km (30 points). Only ordered pairs of data within a regression with an R^2 of more than 0.95 are selected to ensure that the lidar and the radiosonde are sampling the same atmospheric layer. Then, the individual ordered pairs are accepted in the final dataset only if they are included within a percentage of a least mean of squares fit line. If the final dataset is composed of at least 60 points, they are used to calculate the calibration coefficient as the mean of the ratio of the ordered pairs. If the sample does not reach 60 points, the threshold on R^2 is lowered and the accuracy increased. During the MORGANE campaign, the R^2 and the accuracy ranged from 0.80 to 0.97 and from 5 to 20%, respectively, depending on the type of sonde. The final calibration value is the mean ratio between the data of each ordered pair. This method produces a time series of daily calibration coefficients between 15 and 28 May for each type of sonde and for the GNSS (Fig. 4). Only the results for the nights when the water vapor lidar was operating and when radiosounding was performed simultaneously are shown. The mean GNSS calibration coefficient for the selected dates is 159.6 (and its standard deviation ±17.9). The MORGANE campaign is included in IQSP n°11, for which the calibration coefficient is 153.7 (±15.3) (Table 2). The calibration coefficients based on the CFH, RS92 and M10 sondes are 153.6 (±5.9), 161 (±9.2), and 149.8 (±6.4), respectively (Fig. 4). All the mean coefficients derived from the different sondes are included in the standard deviation interval of the GNSS based calculation. The calibration coefficient of IQSP n°11 shows a mean bias of less than 5%, 2.5% and 0.1% with the calibration coefficients derived from the RS92 capacitive sensor technique, from the M10 and from the CFH technique, respectively (Fig. 4). Taking the uncertainties of the different instruments into account, all the techniques are in relatively good agreement. Thus, it is confirmed here that the GNSS technique is as suitable as radiosoundings for the calibration of the water vapor profiles of the Lidar1200. Both techniques show a day-to-day variability (around 5% for the sondes and around 10% for the GNSS). The radiosonde-based calibration technique is supposed to prevent the influence of atmospheric variability (Whiteman et al., 2012). The main source of variability of the calibration might come from the uncertainties of the radiosondes and the GNSS.

2.3.5 Limits of the methodology

The accuracy of the GNSS calibration method is reduced for IWV of less than 10 mm (67% of the number of lidar-coincident IWV) and especially during the dry season. The total column calculated using the vertical profile measured by the CFH sonde and those obtained by GNSS show an average difference of 2 mm. If the CFH is considered as the reference instrument, the uncertainty on the GNSS IWV appears to be around 1-2 mm, which is in agreement with the values of accuracy found in the literature. The calculation of the GNSS IWV uncertainty of the MAIG dataset shows a bias around 1 mm. Figure 5 represents the distribution of the measurements of the GNSS IWV according to the season at the Maïdo Observatory. During summer and autumn, the distributions are more monomodal and imply the largest IWV (30-35 mm). During the winter and the spring, the most common IWV are around 3-5 mm. The austral winter exhibits the driest atmosphere: the IWV can be lower than 3 mm. Thus, the uncertainty on the source of the calibration can be high for a large part of the dataset and during that season in particular. This effect seems to be specific to the subtropical climate regime in the Reunion Island area, where very dry conditions are observed above 5 km altitude from July to September. To avoid too high an uncertainty of the external source of measurement for the calibration, a threshold of 5 mm was chosen for the outliers in the 2013-2015 dataset. One of the main advantages of the use of IQSP is to calibrate those outliers. In the future, the database will be reprocessed with IWV over a shorter temporal resolution, i.e. 10 min, in order to increase the sampling. With a sufficient number of IWV measurements, which remains to be determined, the threshold on the IWV will be increased to 10 mm. This 10 mm threshold will decrease the systematic uncertainty associated with the GNSS IWV in the calibration. Nevertheless, in winter, there might sometimes not be enough IWV values to be taken into account to calculate the calibration coefficient of an IQSP. We expect that, if any change occurs, the continuity will be ensured by the lamp measurements and the monitoring of the instrumental changes via the logbook. Calibration would be improved by launching a few radiosondes in winter from the Maïdo Observatory to confirm, or even determine, the calibration coefficient of the water vapor profiles during these dry conditions. For several years, a radiosounding-based calibration (using the methodology described in Sect. 2.3.3) will support the GNSS-based calibration for the driest months of winter. It will allow us to guarantee the continuity of measurements provided to the networks.

2.3.6 Total uncertainty of the lidar calibration

Calibration coefficients are calculated on the average of the individual hourly coefficients over the quasi-stationary periods. The uncertainty of the calibration coefficient of each period can be estimated by the standard deviation of the hourly coefficients of the associated IQSP. If the calibration is considered as stationary, only subject to random fluctuations, the uncertainty of the calibration coefficient of each period is mainly due to the term corresponding to the standard deviation divided by the square of the number of hourly calibration coefficients. The uncertainty of the transfer of the calibration coefficient varied between 1.6 and 3.1% between 2013 and 2015 (Table 2). The mean standard uncertainty of the dataset is 2.7%. Two systematic uncertainties have to be taken into account regarding the calibration: the uncertainty in the transfer of the calibration from the GNSS to the lidar and the uncertainty of the external source of calibration, i.e. the GNSS IWV described in Sect. 2.3.1.

Transferring the calibration of the GNSS to the Raman lidar entails a systematic uncertainty. Field campaign research shows that this systematic uncertainty is typically 2-5% depending on the particular experiment (Turner et al., 2002; Whiteman et al., 2006; Foth et al., 2015). Introducing 2-5% systematic uncertainties in a time series as an annual change in the calibration would, for example, prevent the detection of trends of 1% per year (magnitude of the water vapor trend in the LS estimated by Rosenlof et al., 2001). Given that time series of lower stratospheric water vapor are desired to be stable at better than 2% per year (GCOS, 2009), the systematic uncertainty associated with the transfer of a calibration from another instrument to the Raman lidar water vapor mixing ratio data product, without considering any other sources of uncertainty, can be sufficient to greatly reduce the value of the time series for lower stratospheric trend detection. This statement is true if the calibration coefficient is assumed to be determined only infrequently (every several months for example), based on comparisons with radiosondes, and carried forward using lamp-based measurements. The way to address this weakness is to perform the dependent calibration frequently enough such that the uncertainty associated with the calibration transfer process becomes part of the random uncertainty budget instead of being part of the systematic uncertainty budget (Whiteman et al., 2011a). This is the technique that the ARM program has followed for its Raman lidars since its inception, by calibrating the water vapor Raman lidar data with respect to microwave radiometer data (Turner et al., 2002). Regarding the Lidar1200, the hourly determination of the calibration coefficient by comparison with GNSS IWV should turn the systematic uncertainty associated with the transfer of calibration from GNSS into a component of the random uncertainty budget. It should also be noted that part of the uncertainty of the GNSS measurement is random (Ning et al., 2013). A detailed calculation of the proportions of random and systematic parts in the total uncertainty of the GNSS might be further investigated. In this paper, the total uncertainty of the GNSS measurement will be considered as a systematic uncertainty for the Lidar1200 profile but the systematic error is probably weaker.

To summarize, an original methodology for Raman lidar calibration has been designed with GNSS measurements. The low values of the standard uncertainty in the transfer of the calibration guarantee high reliability of the calibration coefficient. The methodology minimizes the calibration uncertainty and its use has been successfully tested on the 2-year dataset of the Lidar1200. In the future, a new GNSS IWV dataset will be used: IWV with a temporal resolution of 10 min should soon be available and would ensure a larger sample with more IWV > 10 mm, which would improve the calculation of the calibration coefficient of each IQSP and reduce both systematic and random errors associated with the calibration. The methodology will be further validated through the instrumental comparisons presented in Sect. 3.

3 Validation of the Lidar1200 dataset: comparison with CFH sonde data during measurement campaigns

3.1 Description of the measurement campaigns

The Lidar1200 has been involved in 5 campaigns: MALICCA-1 and 2 in 2013, LIDEOLE-1 in November 2014, MORGANE in May 2015 and LIDEOLE-2 in September 2015. MALICCA-1 (described in Sect. 1) was followed by a complementary campaign, MALICCA-2, during which the last technical details were tested and the instrument was robustly configured for routine measurements. The campaign LIDEOLE-1 focused on the Doppler wind lidar and involved intensive measurements from all lidars at the observatory. A first launch of a CFH sonde was performed in November 2014 and allowed a comparison with the water vapor data of the Raman lidar. The campaign of the largest program in which the Lidar1200 was involved was MORGANE. It took place between 27 April and 29 May 2015, including the technical preparation and the instrumental comparisons. Nine laboratories were involved and about fifteen instruments were operated. The main goals of that campaign were:

- blind comparisons between the temperature, water vapor and ozone lidars of the observatory (Baray et al., 2013) and the NASA/GSFC (Goddard Space Flight Center) STROZ mobile lidar (Leblanc et al., 2011) brought to Reunion Island for the campaign
- daytime and night-time meteorological radiosoundings to work on technical issues associated with GRUAN
- the study of atmospheric processes associated with the composition of the UT/LS and with atmospheric dynamics

Almost 221 hours of acquisition were collected by the lidars of the Maïdo Observatory between 11 and 19 May. A GRUAN exercise with multiple sonde flights (Vaisala, Modem and CFH) was performed during that campaign. After this major campaign, the Lidar1200 was part of LIDEOLE-2. An 8-hour measurement session for the water vapor lidar tested the optimal performances of the instrument on a long-duration session. Within the scope of the evaluation of the performances of the lidar water vapor data, the dataset offered by those campaigns is exceptional, particularly the CFH dataset that will be part of the comparison.

3.2 Presentation of the CFH soundings

Various sondes are used around the world for meteorological radiosoundings. With regard to relative humidity, the CFH and the NOAA frost point hygrometer (FPH) sondes are widely recognized as being among the most accurate, especially in the UT/LS (Hall et al., 2016, Vömel et al., 2007). The CFH is a light balloon-borne hygrometer. The sensor is a mirror chilled by a cryogenic liquid. The principle of the hygrometer is based on the equilibrium between the saturation vapor pressure in the atmosphere and the water (or the ice) at the surface of the mirror at the dew (or frost) point (Oltmans and Hofmann, 1995; Vömel et al., 1995). The instrument adjusts the temperature of the surface to maintain a thin layer of frost water this temperature is the frost or the dew point temperature of the air inside the sensor (Vömel et al., 2007). Using the Goff-Gratch relationship, the water vapor mixing ratio can then be calculated. The uncertainty of the CFH sonde is less than 4% in the lower tropical troposphere, less than 9% in the area of the tropopause and around 10% in the middle atmosphere (around 28 km; Vömel et al., 2007). For the best measurements, the mixing ratio uncertainty can even reach 1% in the lower troposphere and 2 to 3% in the stratosphere (Vömel et al., 2016). After a comparison with the capacitive sensor radiosondes tested in 2010, the last WMO report (WMO, 2011) concluded that only CFH sondes were able to measure the water vapor in the stratosphere.

3.3 Comparison methodology

Six CFH sondes were launched at the Maïdo Observatory during the MORGANE campaign. One of them was launched during the daytime and has not been included in the following comparisons. A methodology of comparison of the data has been developed. For these comparisons, the lidar is calibrated with the GNSS IWV-based methodology described in Sect. 2.3.3. The CFH profiles are smoothed (by applying a 30-point mean filter). For the comparisons in the troposphere, water vapor profiles retrieved by the radiosondes are compared to the 40-min sets of lidar data starting at the launch time of the balloon, except for the 15 May lidar data, for which there was a shift of 11 minutes between the lidar session and the balloon launch due to a delay in starting lidar operations. To compare the profiles in the UT/LS, the time integration for the lidar sessions needs to be expanded. Between 14 and 17 km, the relative difference is minimized if the whole night measurement session of the lidar is used. Above 17 km, it is necessary to involve all the campaign measurements to compare with the mean CFH profile of the campaign. On the other hand, the variability over the 15 days of the campaign seen by the CFH was less than 1 ppmv. Thus, the temporal variability of the water vapor at these altitudes allows an individual profile to be compared with the lidar profile at the scale of the whole campaign. To sum up, in the following, the Lidar1200 integration times used are adjusted with respect to the tropospheric columns analyzed: 40 minutes, night, and the whole campaign (~48 h) for the 2.2-14 km, 14-17 km and 17-22 km partial columns, respectively. These integration times/probed partial column pairs were established to maximize the lidar performances (vertical resolution, uncertainties) in these atmospheric layers following the considerations stated in Sect. 4.

3.4 Results

Figure 6 compares the Lidar1200 and CFH sondes' mean water vapor mixing ratio profiles for the MORGANE campaign. On the left, the mean CFH profile is superimposed on the lidar profile integrated over the whole campaign data in the lower stratosphere (Fig. 6A), on the mean lidar profile of the 40-min sessions in the lower and middle troposphere (Fig. 6B), and on the mean lidar profile of the whole night sessions in the upper troposphere (Fig. 6C). The relative difference between the lidar and CFH profiles is represented on Fig. 6a-c.

In the troposphere, the lidar data used for the comparison represents the average of the five 40-min coincident lidar sessions, while the CFH data is the average of the 5 CFH radiosoundings of the campaign. Good agreement is displayed in the troposphere up to 14 km asl, considering the uncertainties associated with both instruments (Fig. 6C and 6c). The mean relative difference for the 2.2-14 km partial column is about 8.8% and this is much smaller than the variability of the water vapor itself as seen by CFH (Fig. 6c). The relative difference between the CFH and the lidar is characterized by two peaks, at 3 km and around 5 km asl, respectively (Fig. 6c) (both being within the instrument uncertainties, however). All individual comparisons (not shown) agreed similarly, except for the night of 19 May, during which thin water vapor layers observed by the CFH sonde were different (in altitude or in amplitude) from those measured by the Lidar1200. The large spatiotemporal variability of the water vapor is our best scenario to explain the large differences observed on this particular night that does not call into question either the quality of the measurement or the methodology of comparison. The peak at 5 km asl is explained by a persistent sharp water vapor gradient, the altitude of which changes slightly from one day to another and that is seen differently in altitude because of the specific vertical resolution and filtering of the data of each instrument. It just reminds us of the difficulty and highlights the importance of optimizing the instrumental comparison. To conclude, there is very good agreement between the two datasets in the troposphere (2.2-14 km). In the upper troposphere (Fig. 6B and 6b), the lidar data used for the comparison represent the average of the 5 night-sessions coincident with the CFH launches during the campaign. In the lower stratosphere (Fig.6A and 6a), the lidar data used for the comparison represent the integration of the whole 47-hour dataset of the campaign. There is good overall agreement between CFH and Lidar1200 between 14 and 22 km considering the uncertainties of both instruments (Fig. 6A-a and 6B-b). The mean relative difference between the mean CFH and Lidar1200 profiles is 11.4% in the 14-17 km layer (Fig. 6b) and 4.5% in the 17-22 km layer (Fig. 6a), which corresponds to less than 1 ppm. The comparison between the mean profiles shows a bias of more than 10% in the 14-17 km partial column with a peak of around 20% at 15.5 km asl. The durations of the different nightly sessions were not equal, and this fact might have induced some significant differences. Despite this bias, the mean CFH profile is included within the lidar error bar (Fig. 6B). As the spatiotemporal differences increase with the altitude, this remains our best hypothesis to explain the bias.

Below the tropopause (Fig. 6a and 6b), there is a positive bias on the mean lidar data, which can also be found on the comparison with individual profiles. There is no obvious reason for this bias. It may be due to the reduced size of the available sample (5 CFH sondes). Above 22 km (not shown), the CFH and the Lidar1200 are not in agreement. According to the CFH data of this campaign and despite the 47 hours of integration, the Lidar1200 seems to be limited to 22 km asl, probably due to a smaller signal-to-noise ratio above this altitude and/or potential systematic uncertainties. More comparisons will be required to further investigate the reasons for this bias and the altitude of the upper limit for the measurements.

To conclude, the Lidar1200 and the CFH profiles are in good agreement in the troposphere sampled by Lidar1200, except at 3, 5 and 15.5 km asl. The MORGANE campaign profiles have been validated by the CFH sondes up to 22 km asl.

4 Performances of the Lidar1200 in monitoring water vapor

The previous section has demonstrated the agreement between the reference instrument for tropospheric and stratospheric water vapor measurements (CFH) and the Lidar1200. The following section aims to provide an overview of the routine and optimal performances in terms of uncertainties, reachable altitude and vertical resolution.

4.1 Mean performances

To evaluate a mean uncertainty that might be associated with the Lidar1200 water vapor data regarding the altitude, three classes of mean profiles were calculated: all the 10, 40 and 240 minute unfiltered and uncalibrated measurements were averaged. Those classes of profiles were processed with the operating algorithm, associated uncertainties were calculated and a suitable filter was applied (21, 61 and 121 points, respectively). The uncertainty in the transfer of the calibration coefficient is 2.7% (i.e. the standard mean calibration coefficient, Table 2) and the uncertainty of the GNSS measurement is around 11%. Figure 1 represents the different contributions of the uncertainties before filtering and Figure 7 represents the total uncertainty for each class of profiles. As introduced in Sect. 2.2.2, the total uncertainty is influenced by both the calibration and the statistical uncertainties in the lowest troposphere and varies principally under the influence of the statistical uncertainty from the middle troposphere up to the lower stratosphere (Fig. 1). The uncertainty is largely influenced by the integration time and the filtering. Thus, it is important to use a suitable filter to find a good compromise between the vertical resolution and the total uncertainty (cf Sect. 4.4) so that the latter is not too large and does not hide the variability of the water vapor and the magnitude of the processes studied.

The total mean uncertainty for the average profiles of 10, 40 and 240 minutes reaches a threshold of 20% at around 11, 13 and 16 km asl, respectively (Fig. 7). These three classes of profiles provide information on the water vapor mixing ratio in the whole troposphere and offer various time scales for studying atmospheric processes. At 14 km altitude, they present a total uncertainty of 75%, 26% and 13%, respectively (Fig. 7). The 240-min class reaches the tropical tropopause with 25% uncertainty. It appears to be important to reach the tropopause with a smaller uncertainty, and thus to integrate the measurements for longer periods.

Estimating a mean uncertainty in the lower stratosphere is a challenging exercise. With nightly measurements, the stratosphere cannot systematically be reached with an uncertainty lower than 25%; consequently longer integration times are required. One possible solution is to average the lidar signal over several successive nights. Nevertheless, it is difficult to establish homogeneous measurement sessions with around ten hours of integration. If a period of 15 days is randomly selected, except in a campaign mode, it will not be automatically possible for each period to reach 10 hours of measurements. Therefore, a more comprehensive strategy needs to be set up. At present, the investigation of the variability of the water vapor in the UT/LS by lidar is limited to the use of monthly profiles as long as the calibration coefficient can be considered as constant and a long measurement session (8 hours) has been obtained during the one-month period. The Lidar1200 – and the Maïdo Observatory – being designed for long-term operations, the goal here is to build up a database containing monthly UT/LS water vapor profiles over decades. Such a database can be useful to understand climatology and detect long-term trends of UT/LS hydration at this unique subtropical site.

Hoareau et al. (2012) estimated the performances of the Lidar1200 for water vapor measurements based on numerical simulations. They showed that, with 30 minutes of integration, the statistical uncertainty would be 15% at 14.6 km and 30% at 16.3 km and that, with a sufficient number of data, the profiles could reach the stratosphere. The study of the 40-minute average profile for November 2013 – October 2015 (before filtering) shows that, for a statistical uncertainty of 15%, the measurements would reach 9.7 km asl and would rise to 11.1 km asl for 30% (Fig. 1). The total uncertainty (after filtering) would be 15% at 13.1 km asl and 30% at 14.2 km asl (Fig. 7). The simulation of performances by Hoareau et al. (2012) was run for a clear sky, with no moon and using two wavelengths (355 and 532 nm). In practice, the Lidar1200 operates at only one wavelength and for different phases of the moon. The mean profile here was calculated on the whole dataset without taking the moon or the cloud fraction effects into account. The measurement of water vapor during 9 hours in September 2015 showed that the moon phase had a non-negligible influence on the quality of the data (see Sect. 4.2). Using all routine measurement nights (potentially influenced by the moon and variable meteorological conditions), the Lidar1200 shows a total uncertainty of 15% at 14.4 km and 30% at 17.4 km (Fig. 7) for a 240-minute integration time. Four hours of measurement are necessary to reach the upper troposphere.

4.2 Maximum altitude range

In order to estimate the maximum altitude that can be reached for the water vapor profiles in the lower stratosphere, lidar sequences of more than 4 hours are necessary. This is the case only in campaign mode for the Lidar1200. One of the main objectives during the field campaigns (see Sect. 3.1) was to determine the maximum altitude range that could be reached when integrating several nights of measurements. Excluding logistical issues associated with a manually operated lidar and assuming a night with clear sky, the measurement session would exceed ten hours. A test was performed during the LIDEOLE-2 campaign with a night session of about 9 hours. The profile of 24 September 2015 integrated over all-night measurements reached approximately 16 km with an uncertainty of ~30% (~2.5 ppmv). Although the sky was clear, the lidar performance was hampered by the presence of the full moon in the system field of view between 15:00 and 17:00 UTC: between the beginning and end of the measurement session, the sky background on the 387 nm (407 nm) channel increased by a factor of 100 (10). The increase in background affected the first two hours of measurements, limiting those profiles to a maximum altitude of 14 km. Despite this limiting factor, the all-night profile was able to give information on the water vapor up to the tropopause. With lower background noise, it would have most probably reached the lower stratosphere. The factors preventing 10 hours of measurements in a night are various and make this kind of test difficult to implement on a routine basis.

Ten hours is the minimum integration time required to measure up to 18 km with a relative uncertainty of around 35%. The different campaigns allowed us to evaluate the performance of the Lidar1200 in the lower stratosphere in the 18-22 km range (Fig. 8). It would be possible to define an upper limit as the altitude where the lidar uncertainty corresponds to twice the variability of the water vapor in the lower stratosphere. It is noteworthy that the monthly (and even shorter) water vapor variability in the lower stratosphere needs to be further investigated and remains a scientific issue. One value of variability was chosen empirically to illustrate the optimal performance of the Lidar1200. Regarding a 1-ppmv water variability (i.e. 2 ppmv uncertainty), the highest altitude corresponding to the above definition would be 18.1 km asl, 19.5 km asl and 18.5 km asl for 12, 24 and 32 hours of integration, respectively (Fig. 9). The uncertainty on this limit varies between 30 and 40%. By doubling or tripling the integration time, the mean profile could reach a few thousand meters higher with a relative uncertainty of about 35%. At these altitudes, the vertical resolution is 1.3 km. Reliable probing of layers several kilometers above the tropopause has only been possible during the MORGANE campaign, and required about 50 hours of measurements. In this case, the uncertainty in the stratosphere varies between 15 and 23% (at 17 and 22 km asl, respectively, Fig. 9).

The MORGANE campaign profiles highlight the ability of the lidar to retrieve information in the lower stratosphere with a quantified competitive uncertainty. Nevertheless, even if the water vapor can be measured at 18 km with ~10 hours' integration time, the relative uncertainty is high: around 40% for the 9-hour profile. Extending the duration of the integration time to 32 h (50 h) leads to an uncertainty is of 31% (16%) (Fig. 9). These results are in agreement with those of Leblanc et al. (2012), who showed that integration times of 40-70 hours yielded a precision on the lidar measurement equivalent to that of the CFH profiles. The intensive observation periods during the campaigns allow us to obtain more accurate mean results; the stationary character of the water vapor content of air masses is maximized considering the timescale of the water vapor variability above 18 km. The campaigns were organized in spring and autumn and it would be beneficial to have future campaigns in winter and summer.

The performances of the instrument have been defined and the data have been validated, so the database can be used by the scientific community.

4.3 Detection and monitoring of fine-scale structures in the troposphere

One of the key points about the Lidar1200 is its capacity to detect and monitor water vapor structures. Such structures may be signatures of transport and dynamical processes that are interesting to study in the tropical troposphere and lower stratosphere. It is a challenge for the Lidar1200 to retrieve profiles with a high resolution because such structures might be very thin, i.e. around a few hundred meters, with a short lifetime.

Before the MORGANE campaign, a first CFH sonde was launched from the Maïdo Observatory on 18 November 2014. This profiles was not included in the previous validation test because the lidar profile was not valid for a comparison in the upper troposphere because of the failure of one of the laser's chillers. Nevertheless, CFH and lidar water vapor mixing ratio profiles on 18 November 2014 showed good agreement in the troposphere (Fig. 10) and captured an interesting event with respect to the detection of fine-scale structures. The 120-min session lidar profile does not detect the thin water vapor mixing ratio minimum (500 m thickness) included in the thicker wet layer between 8.8 and 10.3 km (Fig. 10 top). Nevertheless, if the lidar data are integrated over only 40- or 30-minute sessions, the minimum is detected (Fig. 10 bottom). This means that fine structures can be smoothed by the data processing if the integration time is not adapted to the lifetime of the processes.

Another comparison was performed on 18 May 2015. A peak of water vapor mixing ratio was located at 9 km asl, with a thickness of 100 m, at 17:16 UTC as observed by a CFH sonde (Fig. 11, black line). This peak was rather poorly captured with the 40-min session lidar data (Fig. 11, red line). In contrast, it was better detected and captured with 10-min session lidar data (Fig. 11). At 17:00 UTC, the lidar already detected a thin wet layer of 400 m and a maximum of 134 ppmv at 9.1 km (Fig. 11, in yellow). This layer was monitored 100 m lower down 10 minutes later, then became thinner and wetter until its characteristics corresponded to the peak observed by the CFH between 17:10 and 17:20 (Fig. 11, in green). Magnitudes of the peak were very similar, 158 ppmv by the lidar versus 180 ppmv by the CFH. The CFH dataset does not give any information on what became of the structure, but the lidar dataset shows that this peak stayed at the same altitude with the same thickness and became drier (Fig. 11, in cyan), dried further, then disappeared (Fig. 11, blue curve). This is an example of the opportunity that the Lidar1200 may provide for fine-scale monitoring of atmospheric structures for geophysical studies.

4.4 Summary

With the benefit of hindsight on the 2-year dataset, it is possible to define an empirical user's guide for the data integration time that leads to a good compromise between uncertainty and vertical resolution (Table 3). Fine-scale structures (vertical thickness of a few hundred meters) can be detected with 10-minute integration profiles. To perform an instrumental comparison in the troposphere with, for example, a radiosonde, an integration time of 40 minutes is necessary. To reach the troposphere above 14 km asl, the integration time should cover at least 4 hours. Around 10 hours of integration are required to reach altitudes above the tropopause with a coarse vertical resolution of ~1.2 km. Depending on the scientific investigations, specific filter points and integration times can be chosen (Table 3). The vertical resolution is coarser in the lower stratosphere but does not exceed 1.3 km. The vertical resolution is below 100 m for profiles of a few minutes (with the number of points of the filter reaching 21) (Fig. 2).

5 Overview of the database and preliminary characterization of seasonal variations of water vapor

5.1 Presentation of the 2-year water vapor database

The 2-year validated water vapor dataset extends from November 2013 to October 2015 (note that the measurements made during the test phase, October 2012 – October 2013, are used internally for specific technical studies). The functioning of the instrument became more stable from November 2013 onward. The number of nights of measurement increased from 66 to 84 nights per year. The number of hours of operation increased by almost 60% year-on-year, from 185 h during November 2013 – October 2014 to 293 h during November 2014 – October 2015. There were 1 to 2 measurement nights per week on average. This dataset includes the routine measurement periods but also Intensive Observing Periods (IOP) during campaigns as described in Sect. 3.1. Efforts to increase the number of measurement sessions on top of IOPs during campaigns ensured that 40% of the measurement sessions in the second year were longer than or equal to 240 min. The proportion of 120-240 min sessions compared to >240 min sessions, respectively 44% and 36% of the whole dataset, and the fact that the most frequent measurement sessions lasted around 240 min show that the time slot of routine operations (i.e. around 19:00 to 01:00 +1 LT) is well covered. The measurements are subject to instrument problems and depend on the availability of the technical staff and, in addition, on meteorological conditions (clear sky nights only). Summer (December-January-February, DJF) is the rainy season with, consequently, the lowest number of measurements. The frequencies of measurements for the other three seasons are similar, although it should be noted that statistics for the March-April-May (MAM) and September-October-November (SON) periods were boosted by the campaigns in November 2013, June 2014 (non-official short campaign), November 2014, and May and September 2015.

5.2 First Maïdo tropospheric seasonal variations of water vapor mixing ratio

A methodology has been established for producing monthly profiles of water vapor mixing ratio. It consists of generating monthly lidar profiles with sessions of 8 hours up to 48 hours, with a calibration coefficient assumed to be unchanged. Data with an uncertainty greater than 80% are not taken into account. These monthly profiles reach the UT with a total uncertainty of less than 18%. Figure 12 shows the time series of monthly water vapor profiles of the Lidar1200 over the 2-year database. Three monthly profiles that do not satisfy the main criterion (i.e. a session of at least 8 hours) have been added to this figure: December 2013, March 2014 and February 2015, with a minimum threshold of 5 hours. Despite the lack of data in January and August, the water vapor seasonal cycle is well documented with the peak of the wet (dry) season in DJF (June-July-August, JJA), which clearly offers hope of further investigating the inter-annual variability and trends with an extended coverage of the database.

Hoareau et al. (2012) had analyzed the profiles obtained between 2002 and 2005 by the instrument in operation in Saint-Denis, before its upgrade and transfer to the Maïdo Observatory, and found a water vapor seasonal cycle from the ground to 9 km characterized by a ratio of (wet seasonal mixing ratio/dry season mixing ratio) between 0.5 and 3. No seasonal cycle was found between 9 and 15 km. The analysis of the new dataset at Maïdo in 2013-2015 confirms a clear seasonal cycle in the lower and middle troposphere. In addition, values in the TTL (Tropical Tropopause Layer) and in the lower stratosphere show some variability, but no seasonal cycle. However, two differences are found with respect to the work of Hoareau et al. (2002):

1. The seasonal cycle is observed higher in the troposphere. Figure 12 shows a clear seasonal variation up to 13 km, as opposed to the 9 km found by Hoareau.
2. Typical monthly values during the wet season are 2000, 200 and 30 ppmv at 5, 10 and 13 km respectively. During the dry season, typical values are 800, 120 and 20 ppmv for the same altitudes.

If we apply the same methodology as Hoareau et al. (2012) and calculate a ratio between the monthly values during the wet (from November to April) and dry (from May to October) seasons, we find values of between 1.5 and 3.7 for this ratio. Ratios above 9 km (between 1.5 and 1.7) are significantly larger than the ratio of 0.4 found by Hoareau et al. (2012). This indicates that the improved technical performance of the system and progress in data processing (especially in the calibration methodology) allow us to better establish the seasonal cycle of water vapor, in terms of difference between the dry and wet seasons and on the vertical range. Future works will be devoted to better characterizing the water vapor variability and associated processes, and long-term trends.

Among some interesting features of this seasonal cycle, Figure 12 shows the great importance of the lowest layer content regarding the total column of water vapor whatever the season, the descent of very dry air below 4 km altitude in JJA, and the occurrence of relative maxima of water vapor mixing ratio above the tropopause (e.g. October 2014, June-July 2015).

6 Conclusion

The spatiotemporal variability of the water vapor in the UT/LS is not well established through direct observations (Kunz et al., 2013; Müller et al., 2016). To fully understand the water vapor variability in the atmosphere, it is necessary to establish climatologies and trends at global and regional scales in the troposphere and in the stratosphere, to characterize the fine-scale structures and to document the associated atmospheric processes. The difficulty in performing these investigations can be found in the collecting of water vapor observations covering the entire atmospheric column (i.e. up to the UT/LS) with an acceptable uncertainty. These data should be obtained regularly over decades with a vertical resolution sufficient to discern the major dynamical processes, and should probe the UT/LS. Establishing such a dataset on several sites worldwide is an important priority for the international networks such as NDACC and GRUAN. These networks require stable instrument systems supplying data with high accuracy, the characterization of the sources of uncertainty, and well documented data processing. Such efforts have been deployed here to produce water vapor profiles using the Lidar1200. In operation at the Maïdo Observatory (Reunion Island) since 2013, this instrument has delivered its first two years of data. The location of Reunion Island, at the edge of both tropical and subtropical latitude bands, makes it possible to study tropical and subtropical mechanisms. Because of the different thermodynamic processes that affect the atmosphere above the South-West Indian Ocean, the water vapor content might show both large and very weak total columns, depending on the season. The significantly dry atmosphere, not only encountered during winter, makes the calibration process very difficult. The different steps to face this challenge and to evaluate the performances of the Lidar1200 have been performed as follows.

- A calibration methodology based on GNSS IWV for long-term stable data processing has been set up.

At the Maïdo Observatory, the GNSS technique is successfully used on a routine basis. The use of GNSS measurements avoids the risk of changes being made to certain instruments by the manufacturer as has occurred with radiosondes in the past. A methodology based on the identification of quasi-stationary periods of the hourly calibration coefficients (i.e. IQSPs) has been applied and tested on the 2013-2015 dataset, allowing a robust calibration of the Lidar1200. A single calibration coefficient is applied to all the data of a given IQSP. Excluding the outliers decreases the uncertainty of the external source of measurement on the calibration. 33% and 67% of the IWV are less than 5 and 10 mm, respectively. A threshold on the IWV value is applied to determine the outliers. The outliers are not taken into account in the calculation of the coefficient but the use of IQSP allows them to be calibrated. Without the IQSP, a large part of this database could not be calibrated. For 2013-2016, the sample was not large enough for a threshold of 10 mm to be applied. Currently, the threshold is 5 mm and is associated with a mean GNSS uncertainty of 11%. The mean standard deviation of the hourly coefficient inside each IQSP is about 10% and the average standard uncertainty on the transfer of the calibration is 2.7%. A comparative methodology has been performed using radiosondes launched simultaneously to the lidar shooting. The calibration technique based on GNSS is in agreement, within 5%, with the mean calibration coefficient calculated by RS92 and shows a mean bias equal of 0.1% when CFH sondes are used for the calibration. The comparative results illustrate the efficiency of this method and are in agreement with the estimation of the uncertainty of the transfer of the calibration from the GNSS to the lidar. Nevertheless, after reprocessing the GNSS database, a threshold of 10 mm (corresponding to a mean total uncertainty of the GNSS of 7.5%) and a minimum size of sample will be taken as criteria for outliers.

- An effort has been made to identify all the significant sources of uncertainty and to assess the total uncertainty budget of the Lidar1200 water vapor measurements.

The main sources of systematic uncertainty are: the calibration, the temperature-dependence of the signal, the overlap function ratios, the correction of the saturation and the differential transmission due to molecules. The systematic component of the total budget uncertainty is driven by the uncertainty of the GNSS measurement. The calibration methodology ensures that this uncertainty is decreased despite the seasonal low water vapor content. The statistical uncertainty increases exponentially with the altitude and dominates in the UT/LS.

- A strategy of data sampling has been deployed to assess the performances of the Lidar1200.

The Lidar1200 mean profiles of 10, 40 and 240 minutes illustrate the total uncertainties that can be achieved in the troposphere. Layers with thicknesses of a few hundred meters can be detected with a temporal resolution of 10 minutes up to around 10 km asl with less than 20% uncertainty. The 240-minute average profile reaches 16 km asl for a total uncertainty of 20%, i.e. a measurement night allows information to be retrieved up to the upper troposphere (subject to good meteorological conditions). The campaigns demonstrate that an integration time of around 10 hours is needed to reach and cross the tropopause. Increasing the range by one kilometer in the lower stratosphere requires an additional 10 to 20 hours, depending on the environmental conditions. The total integration time of 47 hours of the MORGANE campaign allows 22 km asl to be reached with an absolute uncertainty of less than 0.8 ppmv, a relative uncertainty lower than 22% and a vertical resolution of 1.3 km. This evaluation work has led to the creation of a user's guide: the definition of criteria for integration times and filtering adjusted to the process studied in terms of altitude, thickness and temporal scale. The comparison between the results given by CFH sondes launched during MORGANE and the lidar profiles shows that both datasets are in agreement in the troposphere considering the uncertainties of both instruments. The relative difference between the two techniques is even less than the water vapor variability in the troposphere during this period. The positive bias in the 14-17 km range needs to be further investigated. In the UT and in the LS, the absolute difference is lower than 1 ppmv. With respect to the CFH and lidar uncertainties, the instruments are in agreement up to the UT/LS and the CFH profiles validate the lidar data up to 22 km asl. This agreement between the Lidar1200 and the CFH validates the calibration methodology.

Table 3 summarizes the different products that are available and the current associated uncertainties. GRUAN has specific requirements (Table 1) to enable reliable water vapor trend detection in the UT/LS and process studies. The high vertical and temporal resolutions of the Lidar1200 allows fine-scale structures to be studied. The abilities of the Lidar1200 in studying different atmospheric processes such as stratosphere-troposphere exchanges (STE) have already been demonstrated in the literature (Keckhut et al., 2015; Vérèmes et al., 2016). The systematic uncertainty associated with the data of the Lidar1200 in the 2013-2015 database described in this paper is around 10-13%. It includes the uncertainties on the temperature-dependence of the Raman scattering, the overlap ratio and the calibration. To meet the objectives of GRUAN of less than 10% systematic uncertainty, a correction will be applied to the overlap and the threshold of the outliers will be restricted to 10 mm, which will lower the uncertainty of the GNSS to 7.5%, and allow the uncertainty on the transfer of the calibration to be randomized. The random uncertainty for the MORGANE profiles is between 15 and 20% in the UT/LS. The Lidar1200 is able to measure water vapor with an uncertainty of less than 0.8 ppmv.

Some preliminary results have been obtained by analyzing the new dataset at Maïdo in 2013-2015. This analysis confirms a clear seasonal cycle in the lower and middle troposphere. In addition, values in the TTL and in the lower stratosphere show some variability but no seasonal cycle. Some differences with a climatology established by a previous instrument configuration in operation at Saint-Denis in 2002-2005 (Hoareau et al., 2012) have been evidenced, in relation to the vertical range where seasonality can be observed, and to the amplitude of the difference between dry and wet seasons.

To conclude, the Lidar1200 provides water vapor profiles with high vertical and temporal resolution in the troposphere on a routine basis and is able to detect quantities of water vapor of only a few ppmv in the lower tropical stratosphere. The design of the instrument, the excellent measurement environment offered by the Maïdo Observatory, the robustness of the calibration methodology, the transparency on the data processing algorithm, the quantification of the total uncertainty and the instrumental comparison certify the willingness of the Lidar1200 team to respond to the definition of “a reference observation” (Immler et al., 2010). In fact, the water vapor Lidar1200 NDACC application based on the results shown here has recently been positively reviewed by the NDACC steering committee. The Lidar1200 is now able to provide international networks with various routine water vapor data profiles as Level 2 products (based on Table 3), whose use and relevance depend on the user's scientific objectives. A regular effort is made to perform instrumental comparisons through the recurrent CFH soundings performed at the Maïdo Observatory in the GRUAN framework. In addition to its quality, the exceptional character of this dataset resides in its location in the Southern Hemisphere, where it is exposed to dynamical processes associated with tropical and subtropical areas.

Further optimizations of the system are planned to improve the performance of the Lidar1200, especially by upgrading some optical components and cooling the PMT. The technology improvements in the detector might lead to a higher efficiency. A gain of 20% of the signal is estimated to be possible if one of the mirrors is specifically coated for

UV. The stability of the calibration method should be enhanced by using a larger dataset of GNSS IWV. The temporal resolution of the IWV should be lowered to 10 min (against 1 h today). The uncertainty of the calibration should be lowered by increasing the threshold on the IWV to 10 mm, which would decrease the systematic uncertainty associated with the external source of measurement for the calibration. Finally, adaptive or Optimal Estimation Method (OEM) algorithms could be used in an operational way in order to reveal fine-scale structures (Sica and Haefele, 2016; Whiteman et al., 2012), and refine the calculation of the uncertainties and of the calibration coefficient. The use of such a method is part of the future development of the Lidar1200 water vapor data processing intended to bring it closer to the GRUAN requirements. The data of the Lidar1200, used alone and with other measurements performed in Reunion Island, will bring new results on the characterization of water vapor in the troposphere, the monitoring of the water vapor in the UT/LS, the study of the exchange processes between the stratosphere and the troposphere, and the validation of satellite measurements.

Acknowledgments. The Lidar1200 data used in this publication were obtained as part of the Network for the Detection of Atmospheric Composition Change (NDACC) and a level 2 product of daily vertical water vapor profiles will be publicly available through the NDACC portal (http://www.ndacc.org) and the French atmospheric data portal (http://www.pole-ether.fr/). The raw data and other products of the Lidar1200 water vapor data are available at the OPAR web portal (https://opar.univ-reunion.fr/), please contact us or osureunion-informatique@univ-reunion.fr to obtain data download login/password. The ZTD data used to compute the IWV with the GAMIT software were supplied by the OVPF (Observatoire Volcanologique du Piton de la Fournaise).

We acknowledge the ACTRIS project and the support of the European Community (Research Infrastructure Action under the FP7 "Capacities" specific program for Integrating Activities, ACTRIS Grant Agreement no. 262254). The European Commission (FEDER program), Région Réunion and CNRS are acknowledged for their strong support in the building of the Maïdo facility. We are also grateful to Université de La Réunion and CNRS for their strong support of the OPAR station (Observatoire de Physique de l'Atmosphère de La Réunion, UMR8105, UMR8190 and UMS3365) and the OSU-R activities. The authors gratefully acknowledge E. Golubic, P. Hernandez and L. Mottet who are deeply involved in the routine lidar observations at OPAR.

The research leading to these results was supported by the French LEFE INSU-CNRS Program under the projects VAPEURDO and VEGA. We thank the CNRS (Centre National de Recherche Scientifique/France) and the University of Reunion Island for funding the PhD of H. Vérèmes and the MALICCA campaigns.

Thanks are also due to Yann Courcoux, to Jacques Porteneuve, to Alain Hauchecorne, and to Aline Peltier. We are also grateful to Davide Dionisi for his work on the water vapor data processing.

The authors would like to thank the editor, R. J. Sica, and the two reviewers D. N. Whiteman and F. J. Immler whose constructive comments helped considerably in improving the quality of the manuscript.

References

Argall, P. S., Sica, R. J., Bryant, C. R., Algara-Siller, M., and Schijns, H.: Calibration of the Purple Crow Lidar vibrational Raman water-vapour mixing ratio and temperature measurements, Can. J. Phys., vol. 85, no. 2, 119–129, 2007.

Baray, J.-L., Courcoux, Y., Keckhut, P., Portafaix, T., Tulet, P., Cammas, J.-P., Hauchecorne, A., Godin-Beekmann, S., De Mazière, M., Hermans, C., Desmet, F., Sellegri, K., Colomb, A., Ramonet., M., Sciare, J., Vuillemin, C., Hoareau, C., Dionisi, D., Duflot, V., Vérèmes, H., Porteneuve, J., Gabarrot, F., Gaudo, T., Metzger, J.-M., Payen, G., Leclair de Bellevue, J., Barthe, C., Posny, F., Ricaud, P., Abchiche, A., and Delmas, R.: Maïdo observatory: a new high-altitude station facility at Reunion Island (21° S, 55° E) for long-term atmospheric remote sensing and in-situ measurements, Atmos. Meas. Tech., 6, 2865-2877, 2013.

Barnes, J. E., Kaplan, T., Vömel, H., and Read, W. G.: NASA/Aura/Microwave Limb Sounder water vapor validation at Mauna Loa Observatory by Raman lidar, J. Geophys. Res., vol. 113, no. D15, D15S03, 2008.

Bevis, M., Businger, S., Herring, T. A., Rocken, C., Anthes, R. A., and Ware R. H.: GPS meteorology: Remote sensing of atmospheric water vapor using the global positioning system, J. Geophys. Res., vol. 97, no. D14, 15787–15801, 1992.

Bock, O., Bosser, P., Bourcy, T., David, L., Goutail, F., Hoareau, C., Keckhut, P., Legain, D., Pazmino, A., Pelon, J., Pipis, K., Poujol, G., Sarkissian, A., Thom, C., Tournois, G., and Tzanos, D.: Accuracy assessment of water vapour measurements from in situ and remote sensing techniques during the DEMEVAP 2011 campaign at OHP, Atmos. Meas. Tech., vol. 6, no. 10, 2777–2802, 2013.

Bock, O., Bosser, P., Pacione, R., Nuret, M., Fourrié, N., and Parracho, A.: A high-quality reprocessed ground-based GPS dataset for atmospheric process studies, radiosonde and model evaluation, and reanalysis of HyMeX Special Observing Period, Q.J.R. Meteorol. Soc., vol. 142, 56–71, 2016.

Bodeker, G., Bojinski, S., Cimini, D., Dirksen, R., Haeffelin, M., Hannigan, J., Hurst, D., Leblanc, T., Madonna, F., Maturilli, F., Mikalsen, A., Philipona, R., Reale, T., Seidel, D., Tan, D., Thorne, P., Vömel, H., and Wang, J.: Reference upper-air observations for climate: From concept to reality. Bull. Amer. Meteor. Soc., doi:10.1175/BAMS-D-14-00072.1, 2015.

Boers, R., and van Meijgaard, E.: What are the demands on an observational program to detect trends in upper tropospheric water vapor anticipated in the 21st century? Geophys. Res. Lett., vol. 36, no. 19, L19806, 2009.

Bojinski, S., Verstraete, M., Peterson, T. C., Richter, C., Simmons, A., and Zemp, M.: The Concept of Essential Climate Variables in Support of Climate Research, Applications, and Policy, Bull. Amer. Meteor. Soc., vol. 95, no. 9, 1431–1443, 2014.

David, L., Bock, O., Thom, C., Bosser, P., and Pelon, J.: Study and mitigation of calibration factor instabilities in a water vapor Raman lidar, Atmos. Meas. Tech., vol. 10, no. 7, 2745–2758, 2017.

Dionisi, D., Congeduti, F., Liberti, G. L., and Cardillo, F.: Calibration of a Multichannel Water Vapor Raman Lidar through Noncollocated Operational Soundings: Optimization and Characterization of Accuracy and Variability, J. Atmos. Ocean. Tech., vol. 27, no. 1, 2010.

Dionisi, D., Keckhut, P., Courcoux, Y., Hauchecorne, A., Porteneuve, J., Baray, J.-L., Leclair de Bellevue J., Vérèmes, H., Gabarrot, F., Decoupes, R., and Cammas, J.-P.: Water vapor observations up to the lower stratosphere through the Raman lidar during the Maïdo LIdar Calibration Campaign, Atmos. Meas. Tech., 8, 1425-1445, 2015.

Emardson, T. R., and Derks H. J. P.: On the relation between the wet delay and the integrated precipitable water vapour in the European atmosphere, Met. Apps, vol. 7, no. 1, 61–68, 2000.

Foelsche, U. and Kirchengast, G.: Tropospheric water vapor imaging by combination of ground-based and spaceborne

GNSS sounding data, J. Geophys. Res., vol. 106, no. D21, 27221–27231, 2001.

Foth, A., Baars, H., Di Girolamo, P., and Pospichal, B.: Water vapour profiles from Raman lidar automatically calibrated by microwave radiometer data during HOPE, Atmos. Chem. Phys., vol. 15, no. 14, 7753–7763, 2015.

GCOS: The second report on the adequacy of the Global Observing Systems for Climate in support of the UNFCCC, GCOS–82, WMO Tech. Doc. 1143, 85 pages, 2003.

GCOS: GRUAN Implementation Plan 2009-2013, GCOS-134, WMO Tech. Doc. 1506, 54 pages, 2009.

GCOS: The GCOS Reference Upper-Air Network (GRUAN) GUIDE. GCOS-171, Version 1.1.0.3, WIGOS Technical Report No. 2013-03, 116 pages, 2013.

Hall, E. G., Jordan, A. F., Hurst, D. F., Oltmans, S. J., Vömel, H., Kühnreich, B., and Ebert, V.: Advancements, measurement uncertainties, and recent comparisons of the NOAA frost point hygrometer, Atmos. Meas. Tech., 9, 4295-4310, 2016.

Hoareau, C., Keckhut, P., Baray, J.-L., Robert, L., Courcoux, Y., Porteneuve, J., Vömel, H., and Morel, B.: A Raman lidar at La Reunion (20.8° S, 55.5° E) for monitoring water vapour and cirrus distributions in the subtropical upper troposphere: preliminary analyses and description of a future system, Atmos. Meas. Tech., vol. 5, no. 6, 1333–1348, 2012.

Holton, J. R., Haynes, P. H., McIntyre, M. E., Douglass, A. R., Rood, R. B. and Pfister, L.: Stratosphere-troposphere exchange, Rev. Geophys., vol. 33, no. 4, 403–439, 1995.

Hurst, D. F., Read, W. G., Vömel, H., Selkirk, H. B., Rosenlof, K. H., Davis, S. M., Hall, E. G., Jordan, A. F., and Oltmans, S. J.: Recent divergences in stratospheric water vapor measurements by frost point hygrometers and the Aura Microwave Limb Sounder, Atmos. Meas. Tech., 9, 4447-4457, 2016.

Immler, F. J., Dykema, J., Gardiner, T., Whiteman, D. N., Thorne, P. W., and Vömel, H.: Reference Quality Upper-Air Measurements: guidance for developing GRUAN data products, Atmos. Meas. Tech., vol. 3, no. 5, 1217–1231, 2010.

Keckhut, P., Courcoux, Y., Baray, J.-L., Porteneuve, J., Vérèmes, H., Hauchecorne, A., Dionisi, D., Posny, F., Cammas, J.-P., Payen, G., Gabarrot, F., Evan, S., Khaykin, S., Rüfenacht, R., Tschanz, B., Kämpfer, N., Ricaud, P., Abchiche, A., Leclair-de-Bellevue, J., and Duflot, V.: Introduction to the Maïdo Lidar Calibration Campaign dedicated to the validation of upper air meteorological parameters, J. Appl. Remote Sens, vol. 9, no. 1, 094099–094099, 2015.

Kennett, E. J. and Toumi, R.: Temperature dependence of atmospheric moisture lifetime, Geophys. Res. Lett., vol. 32, no. 19, L19806, 2005.

King, R.W., and Bock, Y.: Documentation for the GAMIT analysis software, release 10.32, Massachusetts Institute of Technology, Cambridge, USA, 2007.

Kunz, A., Müller, R, Homonnai, V., Jánosi, I. M., Hurst, D., Rap, A., Forster, P. M., Rohrer, F., Spelten, N., and Riese, M.: Extending water vapor trend observations over Boulder into the tropopause region: Trend uncertainties and resulting radiative forcing, J. Geophys. Res. Atmos., vol. 118, no. 19, 11,269-11,284, 2013.

Kurylo, M. J. and Solomon, S.: Network for the Detection of Stratospheric Change : a status and implementation report, Issued by NASA Upper Atmosphere Research Program and NOAA Climate and Global Change Program, 70 pages, 1990.

Läderach, A. and Sodemann, H.: A revised picture of the atmospheric moisture residence time, Geophys. Res. Lett., 2015GL067449, 2016.

Leblanc, T., Walsh, T. D., McDermid, I. S., Toon, G. C., Blavier, J.-F., Haines, B., Read, W. G., Herman, B., Fetzer, E., Sander, S., Pongetti, T., Whiteman, D. N., McGee, T. G., Twigg, L., Sumnicht, G., Venable, D., Calhoun, M., Dirisu, A., Hurst, D., Jordan, A., Hall, E., Miloshevich, L., Vömel, H., Straub, C., Kampfer, N., Nedoluha, G. E., Gomez, R. M., Holub, K., Gutman, S., Braun, J., Vanhove, T., Stiller, G., and Hauchecorne, A.: Measurements of Humidity in the Atmosphere and Validation Experiments (MOHAVE)-2009: overview of campaign operations and results, Atmos. Meas. Tech., vol. 4, no. 12, 2579–2605, 2011.

Leblanc, T., McDermid, I. S., and Walsh, T. D.: Ground-based water vapor raman lidar measurements up to the upper troposphere and lower stratosphere for long-term monitoring, Atmos. Meas. Tech., vol. 5, no. 1, 17–36, 2012.

Leblanc, T., Sica, R. J., van Gijsel, J. A. E., Godin-Beekmann, S., Haefele, A., Trickl, T., Payen, G., and Gabarrot, F.: Proposed standardized definitions for vertical resolution and uncertainty in the NDACC lidar ozone and temperature algorithms – Part 1: Vertical resolution, Atmos. Meas. Tech., vol. 9, no. 8, 4029–4049, 2016.

Livesey, N. J., Read, W. G., Froidevaux, L., Lambert, A., Manney, G. L., Pumphrey, H. C., Santee, M. L., Schwartz, M. J., Wang, S., Cofield, R. E., Cuddy, D. T., Fuller, R. A., Jarnot, R. F., Jiang, J. H., Knosp, JB. W., Stek, P. C., Wagner, P. A., and Wu, D. L.: EOS MLS Version 3.3 Level 2 data quality and description document, Tech. rep., Jet Propulsion Laboratory, available from http://mls.jpl.nasa.gov/, 2011.

Müller, R., Kunz, A., Hurst, D. F., Rolf, C., Krämer, M., and Riese, M.: The need for accurate long-term measurements of water vapor in the upper troposphere and lower stratosphere with global coverage, Earth's Future, vol. 4, no. 2, 25–32, 2016.

Niell, A. E., Coster, A. J., Solheim, F. S., Mendes, V. B., Toor, P. C., Langley, R. B., and Upham, C. A.: Comparison of Measurements of Atmospheric Wet Delay by Radiosonde, Water Vapor Radiometer, GPS, and VLBI, J. Atmos. Oceanic Technol., vol. 18, no. 6, 830–850, 2001.

Ning, T., Elgered, G., Willén, U., and Johansson J. M.: Evaluation of the atmospheric water vapor content in a regional climate model using ground-based GPS measurements, J. Geophys. Res. Atmos., vol. 118, no. 2, 329–339, 2013.

Ning, T., Wang, J., Elgered, G., Dick, G., Wickert, J., Bradke, M., Sommer, M., Querel, R., and Smale, D.: The uncertainty of the atmospheric integrated water vapour estimated from GNSS observations, Atmos. Meas. Tech., vol. 9, no. 1, 79–92, 2016.

Oltmans, S. J. and Hofmann, D. J.: Increase in lower-stratospheric water vapour at a mid-latitude Northern Hemisphere site from 1981 to 1994, Nature, vol. 374, no. 6518, 146–149, 1995.

Read, W. G., Lambert, A., Bacmeister, J., Cofield, R. E., Christensen, L. E., Cuddy, D. T., Daffer, W. H., Drouin, B. J., Fetzer, E., Froidevaux, L., Fuller, R., Herman, R., Jarnot, R. F., Jiang, J. H., Jiang, Y. B., Kelly, K., Knosp, B. W., Kovalenko, L. J., Livesey, N. J., Liu, H.-C., Manney, G. L., Pickett, H. M., Pumphrey, H. C., Rosenlof, K. H., Sabounchi, X., Santee, M. L., Schwartz, M. J., Snyder, W. V., Stek, P. C., Su, H., Takacs, L. L., Thurstans, R. P., Vömel, H., Wagner, P. A., Waters, J. W., Webster, C. R., Weinstock, E. M., and Wu, D. L. : Aura Microwave Limb Sounder upper tropospheric and lower stratospheric H2O and relative humidity with respect to ice validation, J. Geophys. Res., vol. 112, no. D24, D24S35, 2007.

Rosenlof, K. H., Oltmans, S.J., Kley, D., Russell III, J.M., Chiou, E.-W., Chu, W.P., Johnson, D.G., Kelly, K.K., Michelsen, H.A., Nedoluha, G.E., Remsberg, E.E., Toon, G.C., and McCormick, M.P.: Stratospheric water vapor increases over the past half-century, Geophys. Res. Lett., vol. 28, no. 7, 1195–1198, 2001.

Saastamoinen, J.: Atmospheric Correction for the Troposphere and Stratosphere in Radio Ranging Satellites, in The Use of Artificial Satellites for Geodesy, S. W. Henriksen, Armandoncini, and B. H. Chovitz, Eds. American Geophysical Union, 247–251, 1972.

Seidel, D. J., Berger, F. H., Immler, F., Sommer, M., Vömel, H., Diamond, H. J., Dykema, J., Goodrich, D., Murray, W., Peterson, T., Sisterson, D., Thorne, P., and Wang, J.: Reference Upper-Air Observations for Climate: Rationale, Progress, and Plans, Bull. Amer. Meteor. Soc., vol. 90, no. 3, 361–369, 2009.

Sherlock, V., Hauchecorne, A., and Lenoble, J.: Methodology for the Independent Calibration of Raman Backscatter Water-Vapor Lidar Systems, Applied Optics, vol. 38, no. 27, 5816, 1999a.

Sherlock, V., Garnier, A., Hauchecorne, A., and Keckhut, P.: Implementation and Validation of a Raman Lidar Measurement of Middle and Upper Tropospheric Water Vapor, Applied Optics, vol. 38, no. 27, 5838, 1999b.

Sica, R. J., and Haefele, A.: Retrieval of water vapor mixing ratio from a multiple channel Raman-scatter lidar using an optimal estimation method, Appl. Opt., vol. 55, no. 4, 763–777, 2016.

Solomon, S., Rosenlof, K., Portmann, R., Daniel, J., Davis, S., Sanford, T., and Plattner, G.-K.: Contributions of stratospheric water vapor to decadal changes in the rate of global warming, Science, 327, 1219–1223, 2010.

Trenberth, K. E.: Atmospheric Moisture Residence Times and Cycling: Implications for Rainfall Rates and Climate Change, Climatic Change, vol. 39, no. 4, 667–694, 1998.

Turner, D. D., Linne, H., Bosenberg, J., Lehmann, S., Ertel, K., Goldsmith, J. E. M., and Tooman, T. P.: Simultaneous ground-based remote sensing of water vapor by differential absorption and Raman lidars, in Geoscience and Remote Sensing Symposium, 2000. Proceedings. IGARSS 2000. IEEE 2000 International, 2000, vol. 4, pp. 1455–1458 vol.4, 2000.

Turner, D. D., Ferrare, R. A., Brasseur, L. A. H., Feltz, W. F., and Tooman, T. P.: Automated Retrievals of Water Vapor and Aerosol Profiles from an Operational Raman Lidar, J. Atmos. Oceanic Technol., vol. 19, no. 1, 37–50, 2002.

Venable, D. D., Whiteman, D. N., Calhoun, M. N., Dirisu, A. O., Connell, R.M.. and Landulfo E.: Lamp mapping technique for independent determination of the water vapor mixing ratio calibration factor for a Raman lidar system, Appl. Opt., vol. 50, no. 23, 4622–4632, 2011.

Vérèmes, H., Cammas, J.-P., Baray, J.-L., Keckhut, P., Barthe, C., Posny, F., Tulet, P., Dionisi, D., and Bielli, S.: Multiple subtropical stratospheric intrusions over Reunion Island: Observational, Lagrangian, and Eulerian numerical modeling approaches, *J. Geophys. Res. Atmos.*, 121, 14,414–14,432, 2016.

Vogelmann, H., Sussmann, R., Trickl, T., and Borsdorff, T.: Intercomparison of atmospheric water vapor soundings from the differential absorption lidar (DIAL) and the solar FTIR system on Mt. Zugspitze, Atmos. Meas. Tech., vol. 4, no. 5, 835–841, 2011.

Vogelmann, H., Sussmann, R., Trickl, T., and Reichert, A.: Spatiotemporal variability of water vapor investigated using lidar and FTIR vertical soundings above the Zugspitze, Atmos. Chem. Phys., vol. 15, no. 6, 3135–3148, 2015.

Vömel, H., Oltmans, S. J., Hofmann, D. J., Deshler, T., and Rosen, J. M.: The evolution of the dehydration in the Antarctic stratospheric vortex, J. Geophys. Res., vol. 100, no. D7, 13919–13926, 1995.

Vömel, H., David, D. E., and Smith, K.: Accuracy of tropospheric and stratospheric water vapor measurements by the cryogenic frost point hygrometer: Instrumental details and observations, J. Geophys. Res., vol. 112, no. D8, D08305, 2007.

Vömel, H., Naebert, T., Dirksen, R., and Sommer, M.: An update on the uncertainties of water vapor measurements using cryogenic frost point hygrometers, Atmos. Meas. Tech., vol. 9, no. 8, 3755–3768, 2016.

Wandiger, U.: Raman lidar, in: Weitkamp C., ed., LIDAR: Range-Resolved Optical Remote Sensing of the Atmosphere. Springer, Berlin, p. 241-271, 2005.

Whiteman, D. N.: Examination of the traditional Raman lidar technique. I. Evaluating the temperature-dependent lidar equations, Appl. Opt., vol. 42, no. 15, 2571–2592, 2003.

Whiteman, D. N., Demoz, B., Di Girolamo, P., Comer, J., Veselovskii, I., Evans, K., Wang, Z., Cadirola, M., Rush, K., Schwemmer, G, Gentry, B. Melfi, S. H., Mielke, B., Venable, D., and Van Hove, T.: Raman Lidar Measurements during the International H2O Project. Part I: Instrumentation and Analysis Techniques, J. Atmos. Oceanic Technol., vol. 23, no. 2, 157–169, 2006.

Whiteman, D. N., Vermeesch, K. C., Oman, L. D., and Weatherhead, E. C.: The relative importance of random error and observation frequency in detecting trends in upper tropospheric water vapor, J. Geophys. Res., vol. 116, no. D21, D21118, 2011a.

Whiteman, D. N., Venable, D., and Landulfo, E.: Comments on 'Accuracy of Raman lidar water vapor calibration and its applicability to long-term measurements', Appl Opt, vol. 50, no. 15, 2170-2176; author reply 2177-2178, 2011b.

Whiteman, D. N., : Correction technique for Raman water vapor lidar signal-dependent bias and suitability for water vapor trend monitoring in the upper troposphere, Atmos. Meas. Tech., vol. 5, no. 11, 2893–2916, 2012.

WMO report by Nash, J., Oakley, T., Vömel, H., Wei, Li.: WMO intercomparison of high quality radiosonde systems, Yangjiang, China, 12 July–3 August 2010, WMO Instruments and Observing Methods. Report No. 107, 2011.

Wulfmeyer, V., Hardesty, R. M., Turner, D. D., Behrendt, A., Cadeddu, M. P., Di Girolamo, P., Schlüssel, P., Van Baelen, J., and Zus, F.: A review of the remote sensing of lower tropospheric thermodynamic profiles and its indispensable role for the understanding and the simulation of water and energy cycles, Rev. Geophys., vol. 53, no. 3, p. 2014RG000476, 2015.

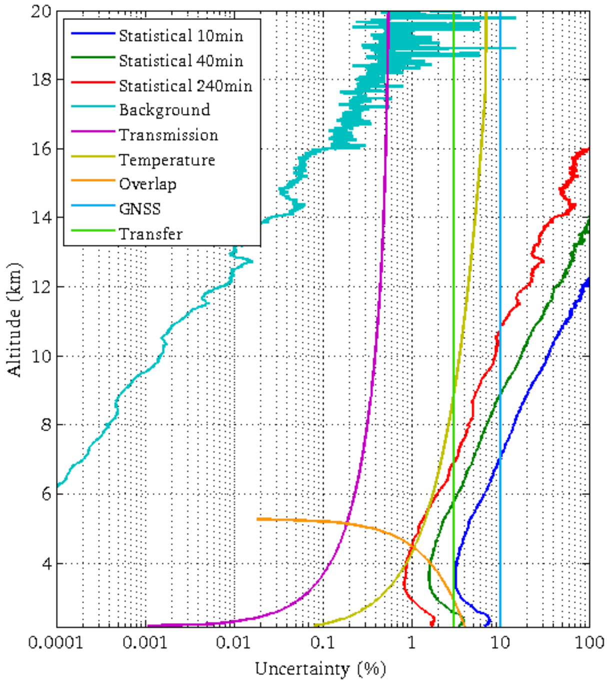

Figure 1. Different systematic uncertainties and random uncertainties for a mean lidar profile integrated over 10 minutes (in blue), 40 minutes (in green) and 240 minutes (in red) according to the altitude above sea level.

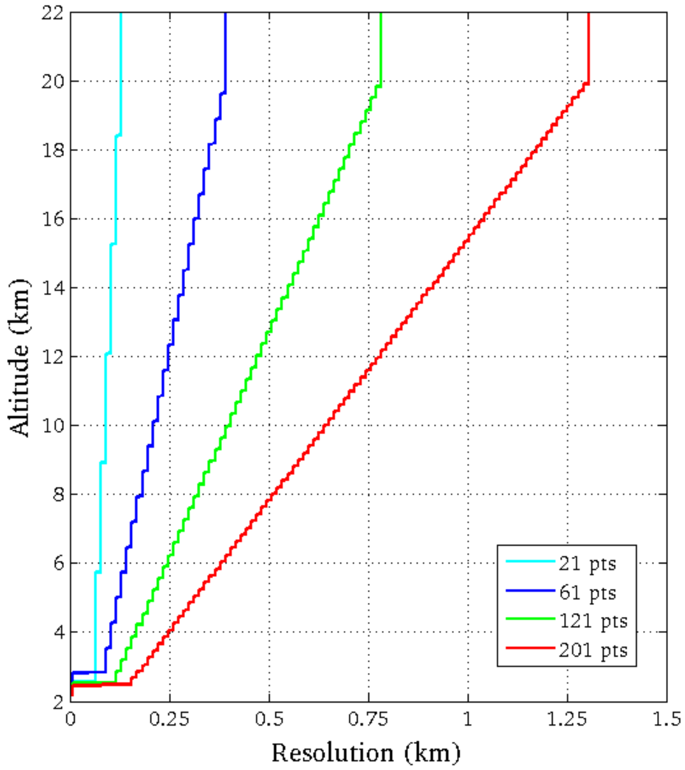

Figure 2. Vertical resolution of the Lidar1200 profile versus altitude (km asl) with respect to the number of points of the filter (Blackman window): 21 points in cyan, 61 in blue, 121 in green and 201 in red, at the altitude of 20 km asl.

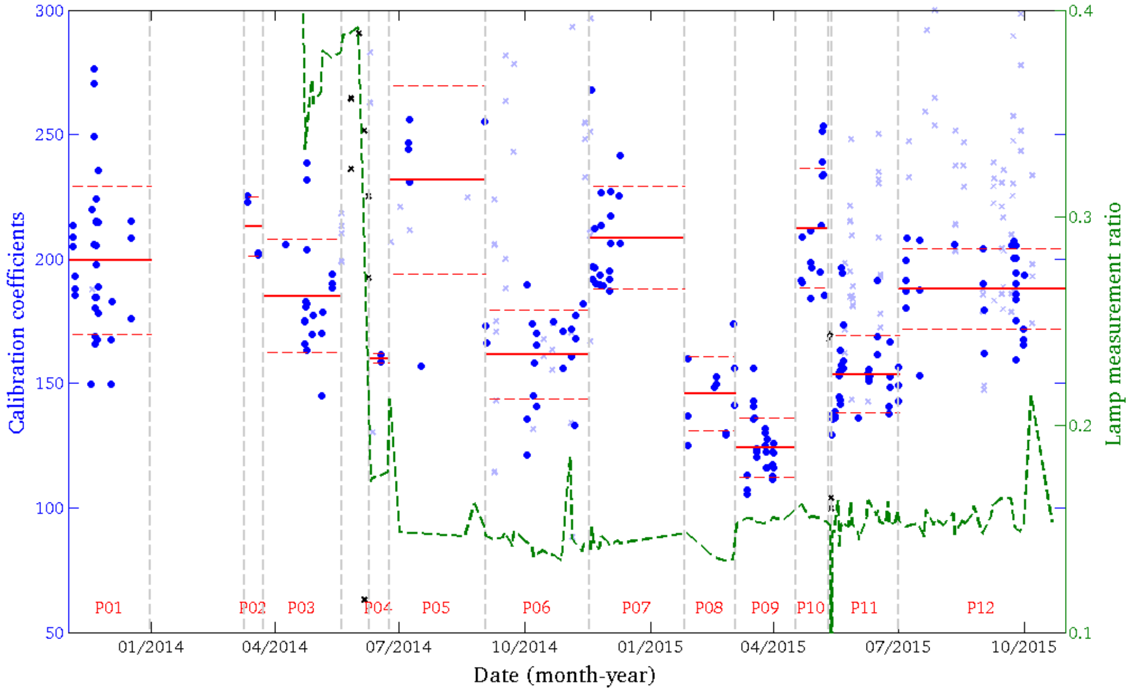

Figure 3. Time series of the hourly coefficients (blue dots and crosses) for the Lidar1200 2-year dataset. The green dotted line corresponds to the lamp measurements made at the beginning of each measurement night from April 2014. The vertical dotted lines separate the twelve quasi-stationary periods (P01 to P12) of the calibration coefficient. Horizontal solid red segments display values of the average hourly coefficient over the corresponding IQSP, i.e. the calibration coefficient. Outliers (sky blue crosses) are not taken into account for the calculation of the average. Black crosses represent measurements that cannot be calibrated within an IQSP. The horizontal dotted red segments correspond to values of the mean hourly coefficients plus or minus the standard deviation.

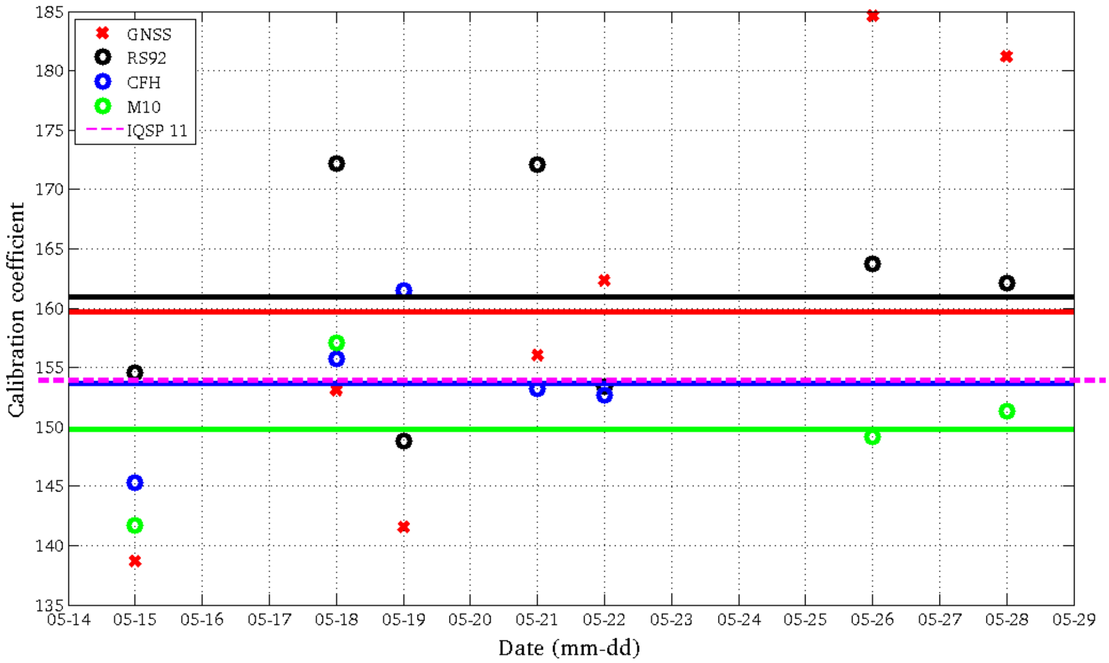

Figure 4. Time series of the Lidar1200's daily coefficients calculated with CFH (blue), RS92 (black), M10 (green), and GNSS IWV (red). The solid lines represent the mean calibration coefficient based on each type of radiosonde measurement during the MORGANE campaign, and the magenta horizontal dotted line represents the calibration coefficient extracted from Table 2.

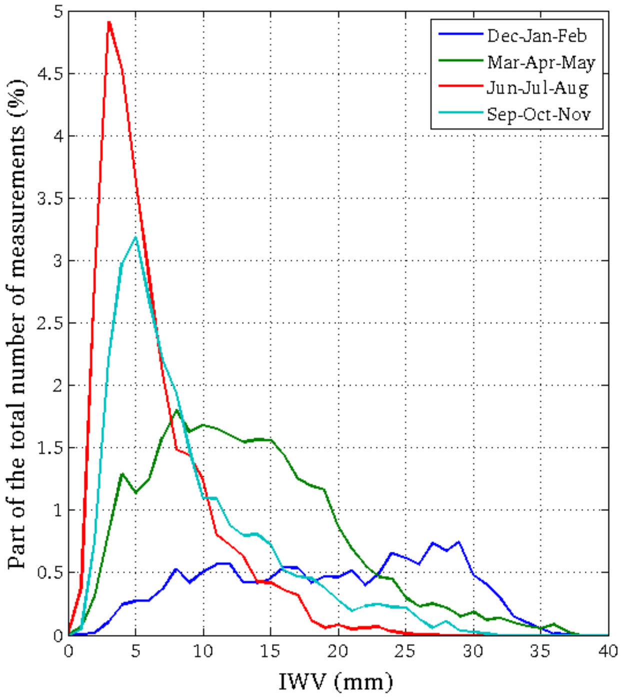

Figure 5. GNSS IWV distribution depending on the total number of measurements by season (in blue for the austral summer, in green for the autumn, in red for winter and in cyan for spring). The 2013-2015 GNSS IWV database includes day and night measurements.

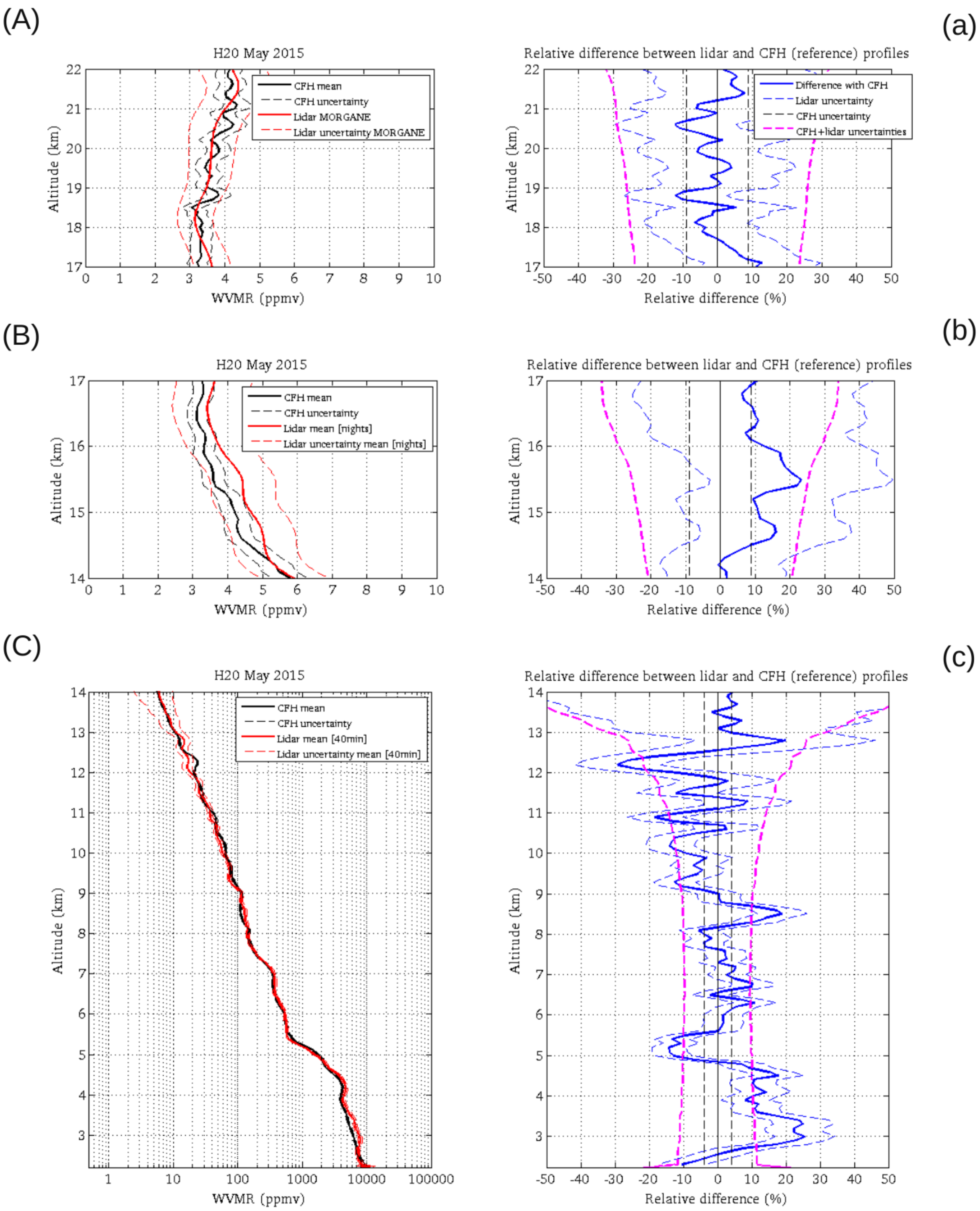

Figure 6. Comparison of the lidar and CFH water vapor mixing ratio during MORGANE between 2.2 km and 22 km. On the left: superimposition of the mean CFH water vapor profile (thick solid black line) with the lidar profile (solid red line). At the bottom: mean profile of the 40-min sessions between 2.2 and 14 km asl, in the middle: mean lidar profile of the night sessions between 14 and 17 km asl and, at the top: the lidar profile integrated over the whole campaign data between 17 and 22 km asl. The red dotted line represents the +/-1σ lidar total uncertainty and the black line represents an uncertainty of the CFH of 4% in the troposphere up to 14 km asl and 9% in the UT/LS. On the right: relative difference (in %) between the lidar and CFH profiles. CFH data are taken as reference. CFH, lidar and the sum of both uncertainties are indicated in black, blue and magenta dotted lines, respectively.

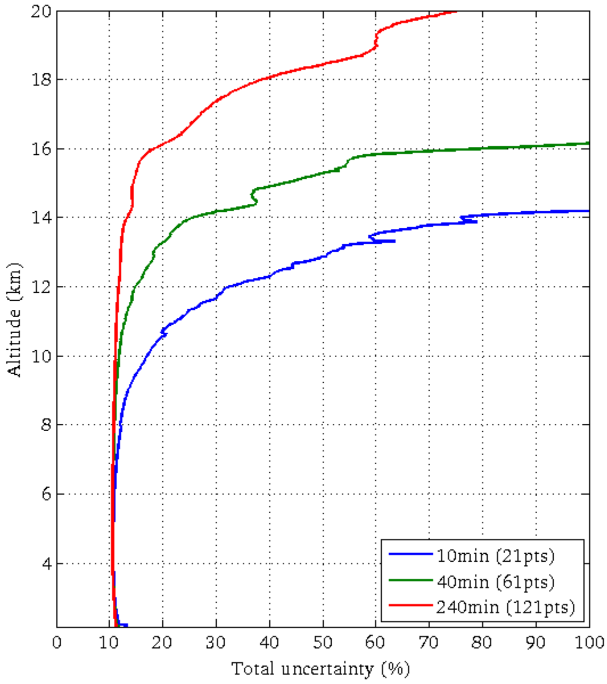

Figure 7. Total uncertainty for a mean lidar profile integrated over 10 minutes (in blue), 40 minutes (in green) and 240 minutes (in red) according to the altitude above sea level.

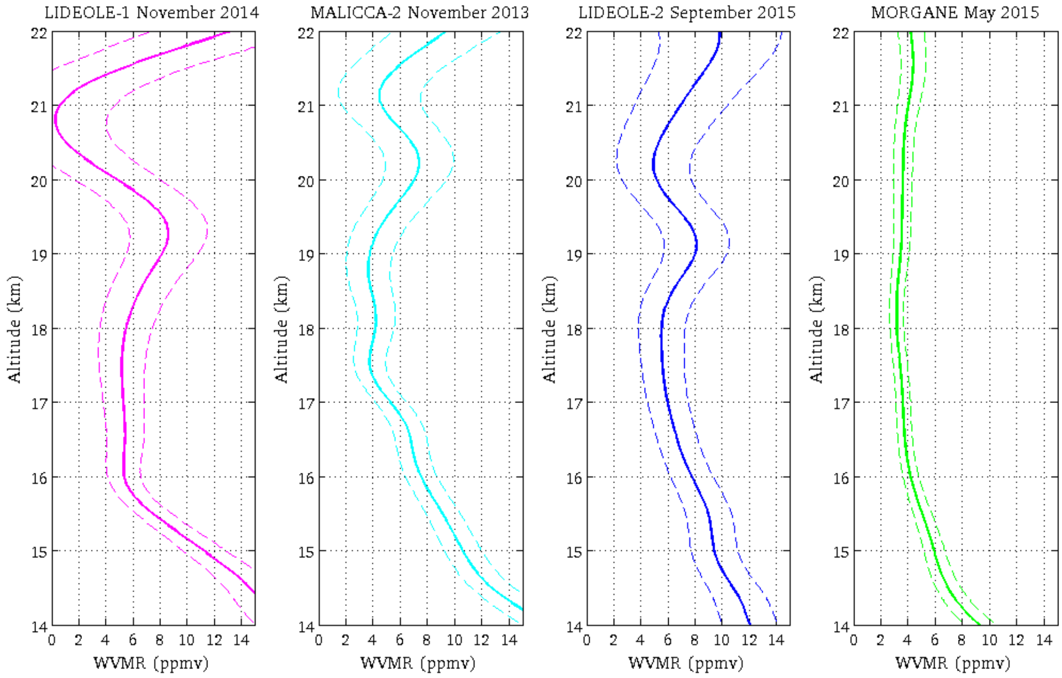

Figure 8. Water vapor mixing ratio profiles integrating all the data of each campaign: LIDEOLE-1 (in magenta) with about 12 h of data, MALICCA-2 (in cyan) with about 24 h of data, LIDEOLE-2 (in blue) with about 32 h of data and MORGANE (in green) with about 47 h of data, between 2.2 and 22 km asl. The dotted lines represent the +/-1σ lidar uncertainty. The filter reaches 201 points.

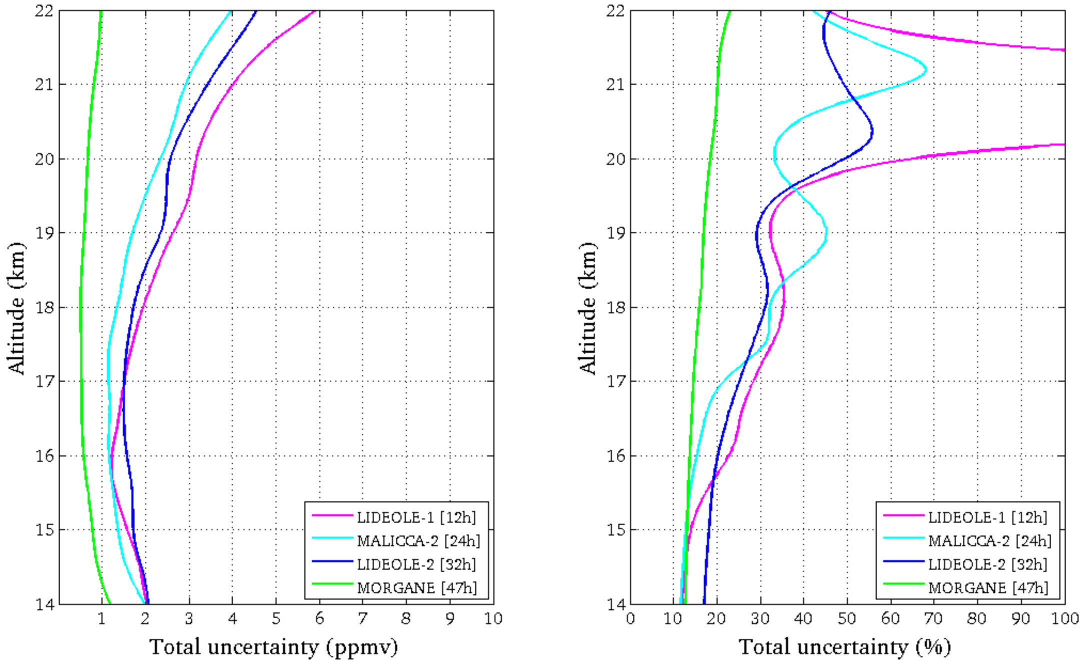

Figure 9. Total uncertainties (on the left: in ppmv, on the right: in %) of the campaign profiles of Figure 8, between 14 and 22 km asl. The colors are the same as in Figure 8.

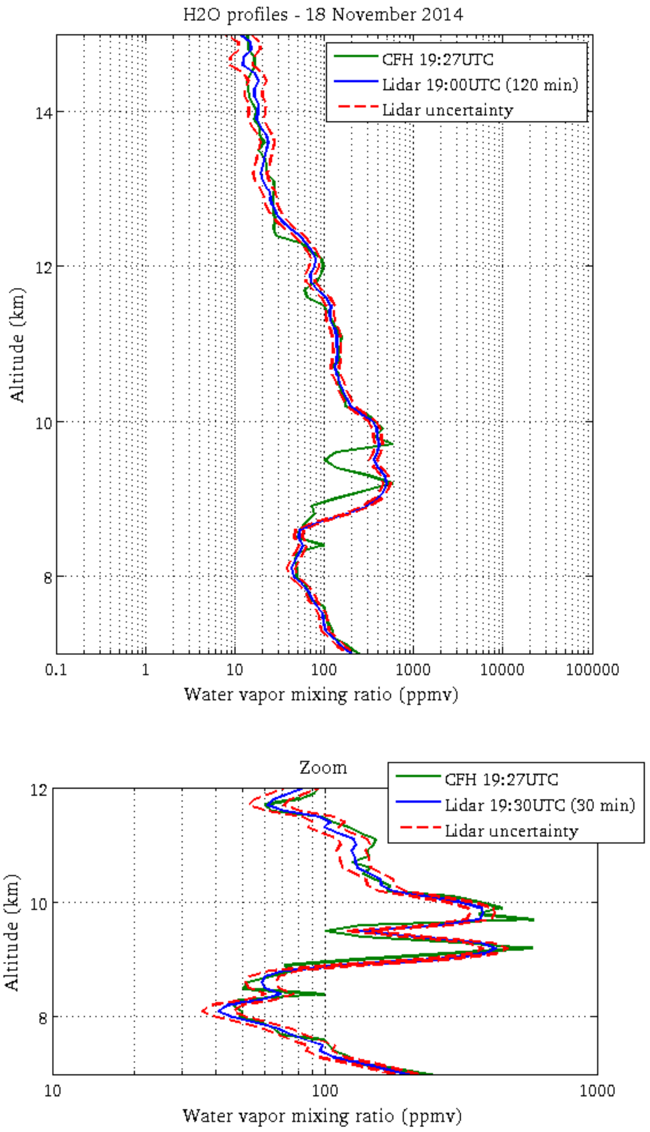

Figure 10. Water vapor mixing ratio profiles on 18 November 2014: CFH sonde (black line, 19:27 UTC) and Lidar1200 profile (in blue) for (top) a 120-min integration (starting at 19:00 UTC) with a 61 point filter between 2.2 and 18 km asl, and (bottom) a 30-min integration (starting at 19:30 UTC) with a 21 point filter between 7.5 and 12 km asl. The red dotted lines represent the +/-1σ lidar total uncertainty.

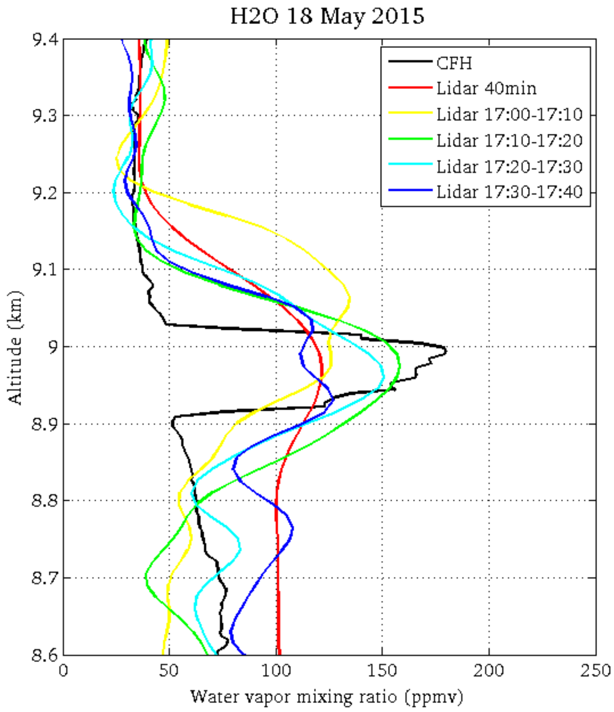

Figure 11. Water vapor mixing ratio profiles on 18 May 2015, CFH (17:16 UTC; in black) and Lidar1200 (17:15 UTC for a 40-min integration in red with a filter of 61 points and by 10-minute steps in colors with a filter of 21 points).

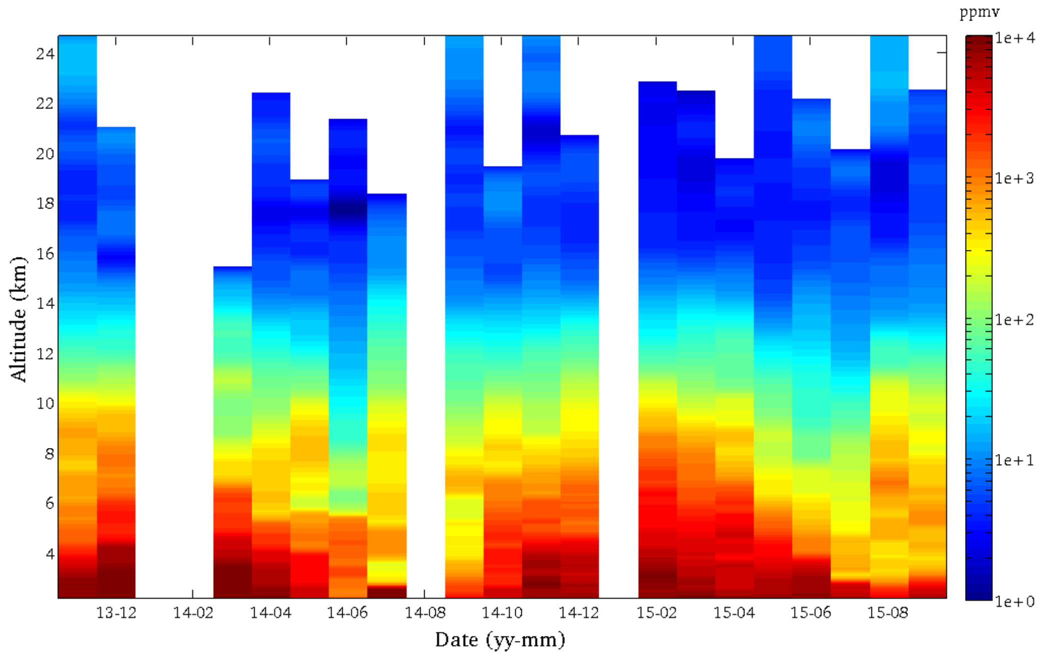

Figure 12. Time series of the water vapor Lidar1200 monthly profiles from November 2013 to October 2015. Lidar sessions of 8-hours minimum are required to build a monthly profile and the data for which the total error is higher than 80% are not taken into account. The threshold has been lowered to 5 hours for three profiles: December 2013, March 2014 and February 2015. The abscissa indicates the year and the month of the profile.

ATTRIBUTE	TREND DETECTION		PROCESS STUDIES
	Upper Troposphere	Lower Stratosphere	
Vertical resolution	< 1 km	< 1 km	10-100 m
Systematic error	5-10%	5-10%	10%
Random error	up to 50%	< 10%	< 10-25%[1]
Stability	no data	no data	N/A
Temporal resolution	< 1 h	no data	1 min

Table 1. GRUAN measurement targets for trend detection and process studies (extracted from GCOS, 2013). [1]Random uncertainty requirements will more likely need to be set by the individual investigators based on their individual needs.

IQSP	DATES	CALIBRATION COEFFICIENT	STANDARD DEVIATION	STANDARD UNCERTAINTY (%)
1	01/11/2013 - 31/12/2013	199	30	2.6
2	10/03/2014 - 23/03/2014	213	12	2.3
3	24/03/2014-19/05/2014	185	23	2.8
4	09/06/2014-23/06/2014	160	2	0.8
5	24/06/2014-01/09/2014	232	37	6.7
6	02/09/2014-16/11/2014	162	18	2.5
7	17/11/2014-25/01/2015	209	20	2.1
8	26/01/2015-03/03/2015	146	15	3.1
9	04/03/2015-08/04/2015	124	12	1.9
10	17/04/2015-10/05/2015	212	24	2.9
11	13/05/2015-30/06/2015	154	15	1.6
12	01/07/2015-31/10/2015	188	16	1.6

Table 2. Chart recapitulating the different calibration coefficients of the water vapor data of the Lidar1200 between November 2013 and October 2015.

<table>
<tr><th>ALTITUDE RANGE (km asl)</th><th>TEMPORAL RESOLUTION (min)</th><th>FILTER (number of points at 21 km)</th><th>VERTICAL RESOLUTION (m)</th><th>SYSTEMATIC UNCERTAINTY (%)</th><th>STATISTICAL UNCERTAINTY (%)</th><th>TOTAL UNCERTAINTY (%)</th></tr>
<tr><td>2.2-10</td><td>10</td><td>21</td><td>65-90</td><td rowspan="4">10-15*</td><td>2.5-15**</td><td>< 20**</td></tr>
<tr><td>2.2-14</td><td>40</td><td>61</td><td>100-300</td><td>2-25**</td><td>< 25**</td></tr>
<tr><td>2.2-17</td><td>240-480</td><td>121</td><td>100-650</td><td>1-25**</td><td>< 30**</td></tr>
<tr><td>2.2-22</td><td>~2800</td><td>201</td><td>150-1300</td><td>< 20**</td><td>< 25**</td></tr>
</table>

Table 3. User's guide for the Lidar1200 water vapor data treatment regarding the altitude range and current associated uncertainties. *The systematic uncertainty includes the uncertainty in the transfer of the calibration that could be randomize. **Corresponds to the random and total uncertainties on the mean signals for 10-, 40- and 240-min integration. The uncertainties for the 2800 min product correspond to the MORGANE results.